

# Nonlinear site response at liquefiable sites: Insights from downhole seismic observations



Weiwei Zhan, Qiushi Chen\*

The Glenn Department of Civil Engineering, Clemson University, Clemson, SC, United States of America

## ARTICLE INFO

**Keywords:**  
 Liquefaction  
 Vertical array  
 Nonlinear site response  
 Strong-motion seismology  
 Ground motion

## ABSTRACT

The nonlinear behavior of shallow soil plays an important role in modifying surface ground motions. We analyze the nonlinear site response at liquefiable sites using the compiled long-term ground motion data (ranging from 1992 to 2020 with over 2000 earthquake events) at four high-quality downhole arrays that have liquefied during at least one earthquake. Two nonlinear event parameters, the percentage of nonlinearity (PNL) and the frequency shift parameter (*fsp*), are used to quantify the modification of site response of strong events to that of weak events. Site-specific regression analyses are performed to correlate nonlinear event parameters to incident motion parameters. Results indicate that site response at liquefiable sites varies from linear to nonlinear to liquefied states as the incident motion intensity changes, and the occurrence of liquefaction could enhance the amplification of low-frequency and very-high-frequency ground motions. As strong-motion observations for liquefiable sites are very limited, the findings of this work are of significance for further study of strong-motion seismology at liquefiable sites.

## 1. Introduction

Earthquake-induced soil liquefaction generates two major concerns: 1) liquefaction may cause excessive ground deformations or ground failures, and 2) liquefaction-induced ground softening may adversely amplify ground motions. While the first item has been extensively studied by the geotechnical earthquake engineering community, the effects of liquefaction on seismic site response are not yet well understood. Seismic observations at liquefied sites have revealed a characteristic waveform composed of intermittent high-frequency spikes riding on a low-frequency carrier (Bonilla et al., 2005; Holzer et al., 1989; Iai et al., 1995; Roten et al., 2013), which has been shown to be related to local site effect (Bonilla et al., 2005). This effect is important for strong-motion seismology as it can change the broadband amplification characteristics, and the liquefaction-induced acceleration spikes can produce large, if not the largest, accelerations (Bonilla et al., 2005). As liquefaction can be considered one state of soil behavior, the understanding and evaluation of site responses at liquefiable sites is of great importance for the earthquake engineering and geotechnical engineering community.

It has been documented that the subsoil liquefaction could affect the characteristics of surface ground motion, alternating both the amplitude

and frequency contents (Zorapapel and Vucetic, 1994). The effects of soil softening and liquefaction on spectral accelerations have been explored in previous studies. For instance, Youd and Carter (2005) compared the recorded ground motions at liquefied sites with predicted ground motions using the equivalent linear site response analysis. Gingery et al. (2015) compared the spectral accelerations of 19 liquefied strong ground motions from shallow crustal earthquakes with the non-liquefied ones estimated using the Next Generation Attenuation Ground Motion Prediction Equations (NGA GMPEs) (Power et al., 2008). These previous studies revealed that soil softening usually amplifies long-period spectral values ( $T > 1.0$  s) due to lengthening of the fundamental site period, which could adversely affect the safety of long-period structures. However, there are limitations in the methodologies adopted in previous studies. The equivalent linear site response analysis used by Youd and Carter (2005) has limited accuracy when the shear strain exceeds 0.1% (Kaklaamanos et al., 2013). The NGA GMPEs used by Gingery et al. (2015) were derived from regional data, and therefore, may have a large bias when applied for ground motion estimation at a specific site. Current seismic design codes (e.g., ASCE (2017)) require site-specific seismic response analysis for liquefiable sites, which is still limited in practice as it requires advanced analysis methods and site-specific data. Advanced effective stress analyses have been used to

\* Corresponding author.

E-mail address: [qiushi@clemson.edu](mailto:qiushi@clemson.edu) (Q. Chen).

predict ground motions at liquefiable sites (e.g., Bonilla et al. (2005); Roten et al. (2013); Yang et al. (2000)), but their applications are limited due to the difficulties in calibrating parameters for complex soil constitutive models.

Nonlinear soil behavior has been shown to modify the amplitude and frequency characteristics of surface ground motions. The amplification factors determined from weak motions (linear site response) are significantly larger than those determined from strong motions (nonlinear site response) at sediment sites observed during the 1989 Loma Prieta earthquake (Aki, 1993). The two most widely known frequency-related characteristics of nonlinear site response are the reduction of high-frequency amplification related to an increase of damping and the shift of resonance frequency to lower values due to the reduction of shear modulus (Bonilla et al., 2005; Dhakal et al., 2019; Régnier et al., 2013). The nonlinear site response is influenced by various parameters related to site condition and seismic loading level (Chávez-García and Kang, 2014; Derras et al., 2020; Rathje et al., 2010; Sgarlato et al., 2011; Yang and Yan, 2009). The degree of nonlinearity can vary greatly from site to site, even in a small region (Frankel et al., 2002; Higashi and Sasatani, 2000).

Empirical site responses are usually evaluated by using the spectral ratio between the simultaneous recordings on sediments and on a nearby rock site (the so-called reference site). The main challenge when applying this technique is the selection of a reliable reference site that should not amplify seismic waves and be close enough to the study site so that the path and source effects remain equivalent for both sites (Régnier et al., 2013). Vertical arrays of accelerometers at both surface and downhole overcome this issue and separate the site effect from source and path effects. Accelerometric data from several liquefied vertical arrays have been used to characterize the shear stress-strain relationship (Elgamal et al., 1996) and the shear wave velocity reduction (Thabet et al., 2008) of liquefied strata. Nonlinear site response has been observed and studied by comparing the Fourier spectral ratios of paired surface and downhole ground motions with different intensity levels for non-liquefied sites (Bonilla et al., 2011; Cultrera et al., 1999; Higashi and Sasatani, 2000; Régnier et al., 2013; Wen et al., 2011) and several liquefied events (Aguirre and Irikura, 1997; Bonilla et al., 2005; Iai et al., 1995; Roten et al., 2013). However, comprehensive analyses of nonlinear site response at liquefiable sites are still limited.

In this work, our goal is to empirically evaluate the site responses at liquefiable sites. We emphasize that liquefaction is one state of nonlinear soil behavior under strong motion excitation and hypothesize that site responses could vary from linear to nonlinear to liquefied (extremely nonlinear) states at liquefiable sites. To test this hypothesis, we evaluate the nonlinear site response at liquefiable sites using long-term ground motion observations at four high-quality downhole arrays that have liquefied during at least one earthquake. Over 2000 earthquake recordings have been collected at these liquefiable sites, and seven of them showed liquefaction effects on seismic site responses. Although most of the recordings in this work are from weak earthquakes that did not cause liquefaction, they are useful in capturing the mean and standard deviation of linear site responses and later nonlinear site response assessment. We compute the borehole spectral ratios between the Fourier amplitude spectrum of the surface and downhole recordings of many earthquake events to quantitatively evaluate the broadband amplification characteristics at liquefiable sites. Although the nonlinear and liquefied site response data are still limited at certain sites due to the lack of strong ground motion observations, our analyses and conclusions are valuable as we have considered multiple liquefiable sites and large numbers of earthquakes from various tectonic environments. Besides, we suggest that our analyses based on real-world and long-term observations can be used to validate the advanced numerical methods for site response assessment at liquefiable sites.

Compared to previous studies, this work differentiates in three substantial ways. First, this work evaluates liquefaction effects on site responses using the Fourier amplitude spectrum (FAS) instead of the 5%

damped pseudo-spectral accelerations (PSA) used in previous studies (Gingery et al., 2015; Youd and Carter, 2005). FAS is better suited than PSA for site response assessment purposes as Fourier transform is a linear operation, which makes it a preferred choice in site response studies (Régnier et al., 2013) as well as in some recent ground-motion modeling work (Bayless and Abrahamson, 2019). In addition, PSA is not a direct representation of the frequency content of ground motions as it is a function of the natural period and damping ratio of the single-degree-of-freedom oscillator. Second, this work quantifies the site response nonlinearity at liquefiable sites using two empirical parameters for nonlinear site response assessment, i.e., the percentage of nonlinearity (PNL) and the frequency shift parameter (*fsp*), which are developed from empirical analyses of ground motions recorded at non-liquefiable sites. Third, the present study develops four site-specific regression models to predict PNL and *fsp* at the four selected sites given input downhole PGAs.

## 2. Vertical arrays and data

For the purpose of this study, we select four vertical arrays that have been reported liquefied during at least one earthquake. They are the Wildlife Liquefaction Array (WLA) in the United States, the Port Island Array (PIA), the Kushiro Port Array (KPA), and the Onahama Port Array (OPA) in Japan. All these arrays have site-specific geotechnical data such as soil type and profile, shear wave velocity, and SPT N-values. We compile long-term (from 1992 to 2020) ground motion data with records from over 2000 earthquake events. Table 1 summarizes the information and data collected for all four arrays, and Table 2 summarizes the information of the liquefaction-triggering events. In addition, maps of earthquake epicenters and plots of earthquake magnitude versus epicentral distance and surface PGA have been included in Appendix A. Details of each vertical array are presented in this section.

### 2.1. Wildlife Liquefaction Array

WLA is located in the Imperial Valley area of California. This area is prone to earthquakes and liquefaction. According to Youd (2005), there were six earthquakes in the past that had reported liquefaction manifestations within 10 km of the WLA. Wildlife Liquefaction Array was originally established by the U.S. Geological Survey (USGS) in 1982 and assigned a station ID of 5210 under the United States National Strong-Motion Network. In 2003–04, the new Wildlife Liquefaction Array was instrumented as part of the U.S. National Science Foundation (NSF) Network for Earthquake Engineering Simulation (NEES) and assigned a station ID of WLA under the University of California Santa Barbara (UCSB) Engineering Seismology Network. These two stations are separated by approximately 70 m (Kishida and Tsai, 2021). Station 5210 was instrumented with two triaxial accelerometers at the ground surface and at a depth of 7.5 m, and six pressure transducers at depths between 2.9 and 12 m (Bennett et al., 1984). Station WLA was instrumented with triaxial accelerometers at 9 locations ranging from the ground surface to 100 m deep, and pressure transducers at 10 locations ranging from the ground surface to 6.23 m deep (Kishida and Tsai, 2021). In this work, we collected two earthquake recordings from Station 5210, which included one liquefaction-triggering earthquake. All the other earthquake recordings are from Station WLA. All recorded data can be downloaded from NEES@UCSB (<http://nees.ucsb.edu/data-portal>). The WLA site consists of: (1) a loose silt layer down to about 2.5 m depth; (2) a loose silty sand layer between 2.5 and 6.8 m in depth; (3) a medium to very stiff silty clay layer between 6.8 and 12 m in depth. The ground-water table was at a depth of approximately 1.5 m (Kramer et al., 2018). The soil layer between 2.5 and 6.8 m is the liquefiable strata (Boulanger et al., 2011). The soil profile, the SPT N-values, and the shear wave velocity profile of the WLA site are shown in Fig. 1. The site  $V_{S30}$  (the time average shear-wave velocity of the top 30 m soil layer) is 177 m/s.

For the WLA site, we collected the ground motion records between

**Table 1**

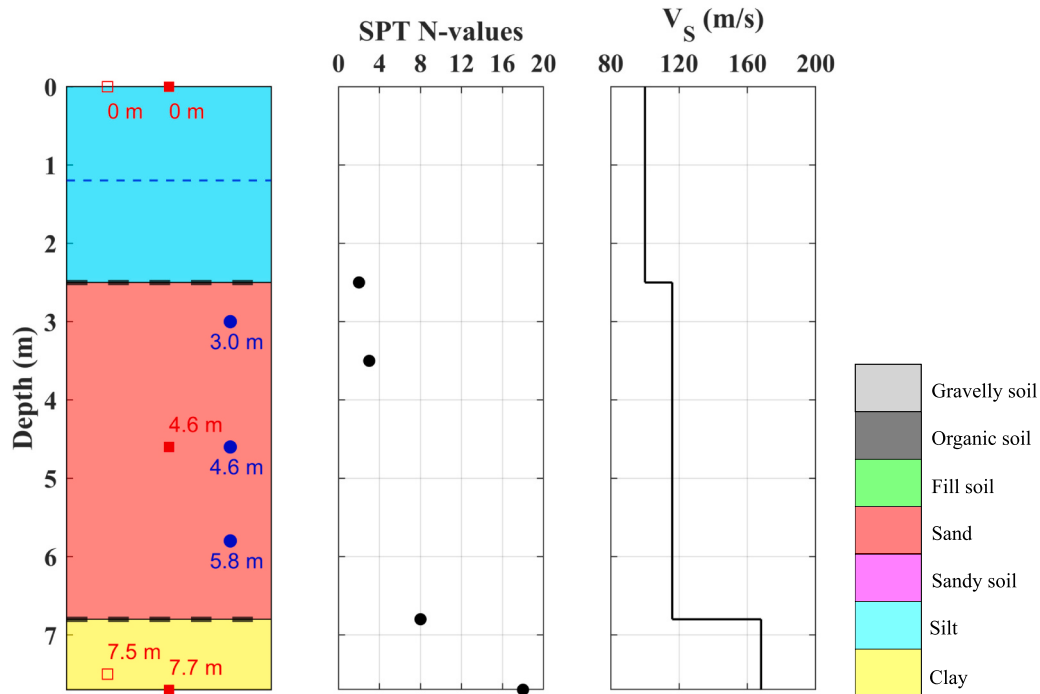
Summary of the site and earthquake information of the four vertical arrays.

Station	$V_{S30}$ (m/s)	Depth (m)	Data period	No. of events	Magnitude <sup>a</sup>	Repi (km)	PGA <sub>surface</sub> (cm/s <sup>2</sup> )		
							min	max	median
WLA	177	7.7	2005~2020	520	3~6.6	5~97	0.4	307.7	4.1
PIA	199	83	1995~2020	189	1.8~9	3~784	0.5	426.4	4.9
KPA	312	77.45	1992~2020	199	3.3~9	5~698	2.5	574.8	10.5
OPA	493 <sup>b</sup>	11.05	1995~2020	1238	2.4~9	4~1252	0.6	1793	4.4

<sup>a</sup>  $M_w$  magnitude for WLA,  $M_{JMA}$  magnitude for the other three sites;<sup>b</sup> The average shear wave velocity of the top 11 m soil.**Table 2**

Summary of the earthquake and liquefaction information of the liquefaction-triggering events at the four vertical arrays.

ID	Station	Event name	Liquefaction evidence	Liquefaction reference	PGA <sub>downhole</sub> (cm/s <sup>2</sup> )	PGA <sub>surface</sub> (cm/s <sup>2</sup> )	PNL	fsp
1	WLA	1987 $M_w$ 6.6 Superstition Hills	Extensive sand boils and recorded high pore water pressure	Holzer et al. (1989)	175.5	206.6	25.7	0.80
	PIA	1995 $M_{JMA}$ 7.3 Hyogoken-Nanbu	Sand ejecta continued one hour after the majorshock	Yamazaki et al. (1995)	723.2	426.4	28.5	0.01
	PIA	1995 $M_{JMA}$ 5.0 aftershock	Sand ejecta continued one hour after the majorshock	Yamazaki et al. (1995)	165.6	38.6	35.4	0.51
	KPA	1993 $M_{JMA}$ 7.6 Kushiro-Oki	Cyclic mobility acceleration spike	Kostadinov and Yamazaki (2001)	276.9	470.3	28.7	0.53
	KPA	1994 $M_{JMA}$ 8.2 Hokkaido Toho-Oki	Soil shear wave velocities reduction from inverse analysis	Thabet et al. (2008)	115.6	274.1	24.9	0.64
	KPA	2003 $M_{JMA}$ 8.0 Tokachi-Oki	Soil shear wave velocities reduction from inverse analysis	Thabet et al. (2008)	229.5	574.8	27.8	0.56
	OPA	2011 $M_{JMA}$ 9.0 Tohoku	Sand boils	Kramer et al. (2016)	196.8	1793.4	21.1	0.25

**Fig. 1.** Wildlife Liquefaction Array profile showing the soil column and depths of sensors, SPT N-values, and the shear wave velocity profile. Accelerometers before 1987, accelerometers after 2001, and pore-pressure transducers are marked as open squares, solid squares, and solid circles, respectively. The liquefiable layer is marked by the two black dashed lines.

2005 and 2020 with a moment magnitude ( $M_w$ ) higher than 3 and an epicentral distance (Repi) smaller than 100 km. In addition, we collected the ground motion records of the two strong earthquakes that occurred in 1987, i.e., the 23 November 1987  $M_w$  6.2 Elmore Ranch earthquake and the 24 November 1987  $M_w$  6.6 Superstition Hills earthquake. Other pre-2005 records are not available for the WLA site. In total, we

collected 520 ground motion records at WLA. The WLA site has recorded three strong ground motions with the downhole peak ground acceleration (PGA<sub>downhole</sub>) exceeding 100 cm/s<sup>2</sup>, one from the 1987 Superstition Hills event and two from the 2012 Brawley swarm. Among these events, the 1987 Superstition Hills event did trigger liquefaction at WLA, where ground cracks and sand boils were observed, and the pore water

pressure ratio was recorded by one piezometer located at 2.9 m depth reached 1.0 (Kramer et al., 2018). Two events of the 2012 Brawley swarm that occurred 20 km southeast of the WLA site produced high pore water pressure at the WLA site but not high enough to trigger liquefaction (Steidl et al., 2014). The ground motions of the Brawley swarm at the WLA site were dominated by a single, high-frequency pulse followed by several seconds of weaker shaking (Kramer et al., 2018). The M 4.9 event that occurred on 27 August 2012 induced a surface peak ground acceleration ( $\text{PGA}_{\text{surface}}$ ) of 307.7 cm/s $^2$  (the corresponding  $\text{PGA}_{\text{downhole}}$  of 277.1 cm/s $^2$ ) and a pore water pressure of 21 kPa (the pore water pressure ratio close to 0.4). The M 4.6 event that occurred on 26 August 2012 induced a surface PGA of 286.3 cm/s $^2$  (the corresponding  $\text{PGA}_{\text{downhole}}$  of 220.2 cm/s $^2$ ) and a pore water pressure of 9.6 kPa (the pore water pressure ratio of 0.2).

## 2.2. Port Island Array

PIA was installed at a reclaimed island by the Development Division of Kobe city in 1991. The seismic observation data of the PIA is distributed by the Port and Airport Research Institute (PARI), Japan. The array consists of four triaxial accelerometers located at the surface, 16 m, 32 m, and 83 m in depths. The site consists of: (1) a reclaimed loose surface layer down to about 19 m in depth; (2) an alluvial clay layer between 19 and 27 m in depth; (3) sand with gravel strata interlayered with clay between 27 and 61 m in depth; (4) a diluvial clay layer between 61 and 82 m in depth; and (5) sand with gravel layers interlayered with clay starting at about 82 m in depth. The water table is located approximately 4 m below the ground surface. Soil layers within 5~16 m depth are liquefiable (Aguirre and Irikura, 1997).  $V_{S30}$  of the PIA site is 199 m/s. The soil profile, the SPT N-values, and the shear wave velocity profile of the PIA site are shown in Fig. 2.

For the PIA site, we collected all the ground motions recorded between 1995 and 2020. The PIA site has recorded two strong ground motions with  $\text{PGA}_{\text{downhole}}$  exceeding 100 cm/s $^2$ , one from the 17 January 1995 M<sub>JMA</sub> 7.3 Hyogoken-Nanbu earthquake and one from its aftershock. The 1995 Hyogoken-Nanbu event induced the largest ground motion at PIA over the instrumented period and triggered

liquefaction (Yamazaki et al., 1995). The second-largest ground motion was induced by an M<sub>JMA</sub> 5.0 aftershock that occurred about seven minutes after the major shock of the 1995 Hyogoken-Nanbu earthquake. The wave propagation of this aftershock was influenced by the liquefied subsoil as sand ejecta continued at the site one hour after the earthquake (Yamazaki et al., 1995). We label this aftershock motion as a post-liquefied motion and will analyze and discuss the effect of liquefied subsoil on site response. Other ground motions recorded at PIA have  $\text{PGA}_{\text{downhole}}$  are less than 100 cm/s $^2$ , among which the largest one was from an M<sub>JMA</sub> 6.3 event that occurred on 12 April 2013 and had a  $\text{PGA}_{\text{downhole}}$  of 66.3 cm/s $^2$ .

## 2.3. Kushiro Port Array

KPA is located in eastern Hokkaido, Japan. This area is prone to earthquakes and liquefaction (Higashi and Sasatani, 2000; Thabet et al., 2008). This array consists of triaxial accelerometers located at the surface and 77.45 m depth. The site lithology can be divided into four main units: (1) a coarse sand layer interlayered with thin sandy gravel layers (0~22 m in depth); (2) a fine sand layer interlayered with silt layers (22~46 m in depth); (3) a sandy gravel layer interlayered with a coarse sand layer (46~52 m in depth); (4) a fine sand layer interlayered with coarse sand layers (52~77.45 m in depth).  $V_{S30}$  of the KPA site is 312 m/s. Soil layers within 6~23 m depth are liquefiable (Thabet et al., 2008). The detailed soil profile, the SPT N-values, and the shear wave velocity profile are shown in Fig. 3.

For the KPA site, we collected a total of 199 sets of ground motions recorded between 1992 and 2020. The magnitude of the recorded earthquakes ranges from M<sub>JMA</sub> 3.3 to 9.0. The KPA site has recorded four strong ground motions with a  $\text{PGA}_{\text{downhole}}$  exceeding 100 cm/s $^2$ , which were from the mainshocks of the 15 January 1993 M<sub>JMA</sub> 7.5 Kushiro-Oki, the 4 October 1994 M<sub>JMA</sub> 8.2 Hokkaido Toho-Oki, the 26 September 2003 M<sub>JMA</sub> 8 Tokachi-Oki, and the 29 November 2004 M<sub>JMA</sub> 7.1 Hokkaido earthquakes. The first liquefaction observation at KPA after the instrumentation was from the 1993 Kushiro-Oki event. Although no surface manifestation of liquefaction was reported during this event, the KIA site was interpreted as liquefied by many researchers

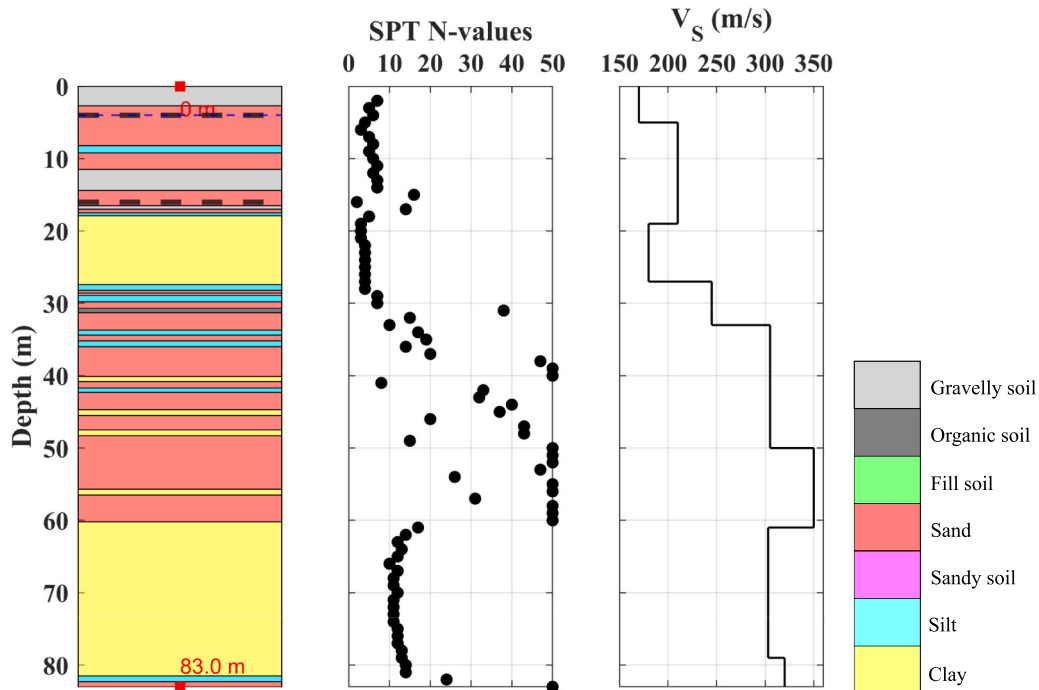


**Fig. 2.** Port Island Array profile showing the soil column and depths of sensors, SPT N-values, and the shear wave velocity profile. Accelerometers are marked as solid squares. The liquefiable layer is marked by the two black dashed lines.

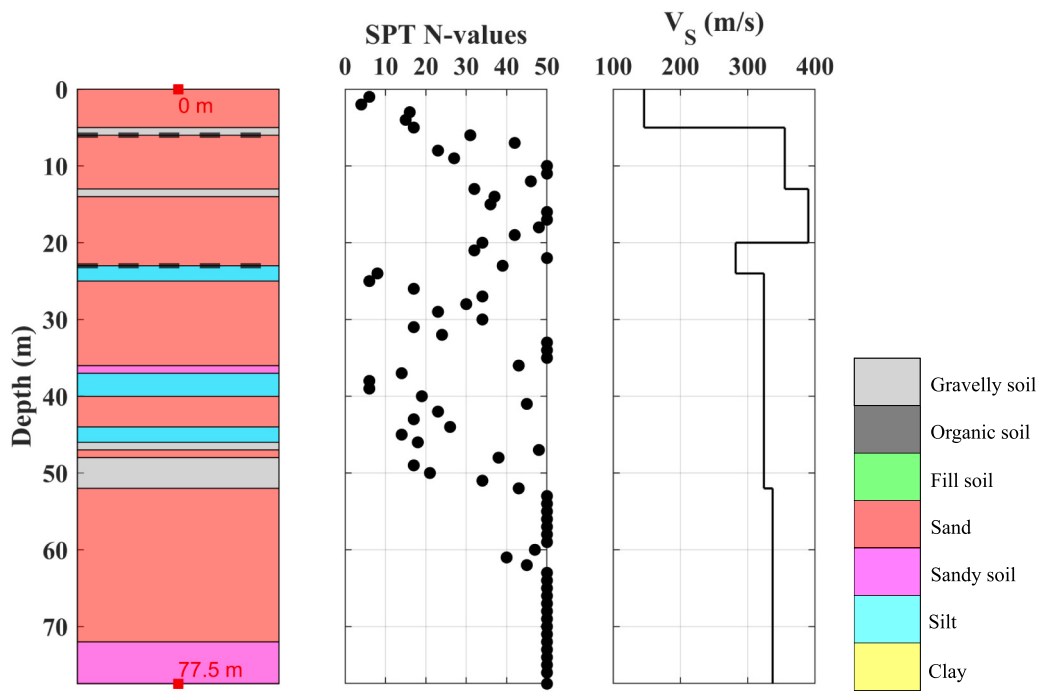


**Fig. 3.** Kushiro Port Array profile showing soil column and depths of sensors, SPT N-values, and shear wave velocities. Accelerometers are marked as solid squares. The liquefiable layer is marked by the two black dashed lines.

since clear cyclic mobility acceleration spikes with a period of about 1.5 s were found in its surface ground motion records (Iai et al., 1994; Kramer et al., 2015; Yamazaki et al., 1995). Based on reductions of shear wave velocities from the inverse analysis, Thabet et al. (2008) suggested the 1993 Kushiro-Oki and the 1994 Hokkaido Toho-Oki events induced a strong degree of liquefaction while the 2003 Tokachi-Oki event induced a low degree of liquefaction. The 2004 M<sub>JMA</sub> 7.1 Hokkaido earthquake did not trigger liquefaction at the KPA site.

#### 2.4. Onahama Port Array

OPA is located near Iwaki City in the Fukushima Prefecture, Japan. This array consists of triaxial accelerometers located at the surface and 11 m depth. The site lithology consists of (1) a reclaimed loose surface layer down to 1.3 m in depth; (2) a dense sand layer between 1.3 and 7 m in depth; (3) a silt layer between 7 and 11 m in depth. With the groundwater level at 1.2 m, the saturated sandy layer (1.3 to 3.0 m

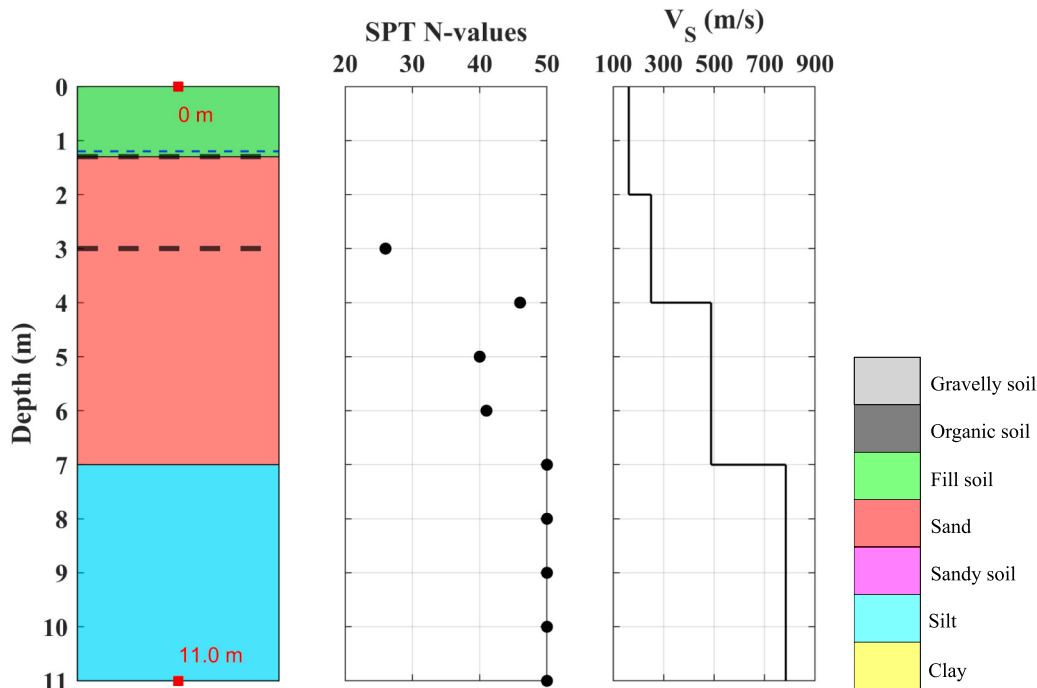


**Fig. 4.** Onahama Port Array profile showing soil column and depths of sensors, SPT N-values, and shear wave velocities. Accelerometers are marked as solid squares. The liquefiable layer is marked by the two black dashed lines.

depth) is liquefiable and is both underlain and overlain by permeable soils (Kramer et al., 2016). The average shear wave velocity of the top 11 m soil ( $V_{11}$ ) at the OPA site is 493 m/s. The detailed soil profile, the SPT N-values, and the shear wave velocity profile are shown in Fig. 4.

For the OPA site, we collected all ground motions recorded between 1995 and 2020. In total, we obtained 1238 pairs of ground motion records. The OPA site recorded three strong ground motions with a  $\text{PGA}_{\text{downhole}}$  exceeding 100 cm/s<sup>2</sup>, which were from the mainshocks of the 11 March 2011 M<sub>w</sub> 9.0 Tohoku earthquake, the 20 September 2013 M<sub>JMA</sub> 5.9 Eastern Honshu earthquake, and the 22 November 2016 M<sub>JMA</sub> 7.4 Fukushima earthquake. The 2011 Tohoku earthquake induced the strongest ground motions, which led to the only liquefaction observation at the OPA site over the instrumentation period. This event caused ground settlement at the Onahama Port. While the port was affected by a tsunami, sand boils were observed from aftershocks (Kramer et al., 2016).

### 3. Methodology for quantifying nonlinear site response

With the site and earthquake information compiled for the four vertical arrays, in this section, we present the methodology for quantifying the nonlinear site responses at those liquefiable sites. The borehole spectral ratio (BSR) will be calculated and used to present the response of each site subjected to an input ground motion. Two nonlinear event parameters will then be defined to characterize the modifications of different earthquake events to the linear site response curve characterized by BSR of the weak motions.

#### 3.1. Borehole spectral ratio and linear site response

In this study, we first use a two-step procedure to pre-process the collected ground motion data to create the surface and downhole acceleration time histories for each earthquake event. The first step is to determine the arrivals of different seismic phases in a waveform using the deep learning-enabled generalized phase detection (GPD) method (Ross et al., 2018), which is able to detect the P-wave and S-wave arrivals, the signal end, and the pre-event noise. If several events are detected in the same waveform, the most energetic one is selected. All seismic phase arrivals are also manually checked and corrected if needed. The second step is to apply a baseline correction to the acceleration time histories selected in the first step. The correction is done by subtracting the mean value from the raw acceleration time history, which will remove an overall offset in the acceleration signal.

We then compute the borehole spectral ratio (BSR), defined as the ratio between the geometric average of the Fourier amplitude spectra of the horizontal ground motion components recorded at the surface and downhole according to Eq. (1):

$$\text{BSR}(f) = \sqrt{\frac{\text{FAS}_{\text{EW},\text{surface}}^2 + \text{FAS}_{\text{NS},\text{surface}}^2}{\text{FAS}_{\text{EW},\text{downhole}}^2 + \text{FAS}_{\text{NS},\text{downhole}}^2}} \quad (1)$$

where  $\text{FAS}_{\text{EW},\text{surface}}$ ,  $\text{FAS}_{\text{NS},\text{surface}}$ ,  $\text{FAS}_{\text{EW},\text{downhole}}$ ,  $\text{FAS}_{\text{NS},\text{downhole}}$  are the smoothed Fourier amplitude spectrum of the East-West, and North-South horizontal components of the surface and downhole recordings, respectively. There are several downhole accelerometers at the WLA and PIA sites. For the BSR calculation, we selected ground motions recorded by the 7.5 m depth and 83 m depth accelerometers at the WLA and PIA sites, respectively, which are below the liquefied layer of each site. To avoid zero values at the denominator of Eq. (1), we apply the Konno-Ohmachi smoothing (Konno and Ohmachi, 1998) with the parameter  $b$  equal to 40 to smooth each Fourier amplitude spectrum (Régnier et al., 2016). To reduce the influence of signal noise on the site response calculation, we calculate BSR at frequencies for which the signal-to-noise ratio is higher than 3.

With BSRs computed, we then characterize the empirical linear site

response at each site, which is represented by the mean and standard deviation (in log unit) of the BSRs computed with recordings of weak motions (surface PGA less than 25 cm/s<sup>2</sup>) (Régnier et al., 2016). The mean empirical linear site response is noted as  $\text{BSR}_{\text{linear}}$ , and its 95% confidence limits are noted as  $\text{BSR}_{\text{linear}}^{95}$ . The variability of BSR at the linear stage is due to source and path effects associated with complex site responses (Régnier et al., 2013). The complexity of the site response may be caused by several factors, such as non-1D site configuration or material anisotropy (Régnier et al., 2013). However, the linear characterization, performed with a large number of recordings, is supposed to contain all the variability, and the difference between site responses computed from strong motions and the linear site response is mostly due to nonlinear soil behavior (Régnier et al., 2013). To quantify the effect of the nonlinear soil behavior on empirical site responses (in terms of the BSR curve), we use two nonlinear event parameters and will detail their calculations in the next sections.

#### 3.2. Nonlinear event parameter: PNL

##### 3.2.1. Definition of PNL

The first nonlinear event parameter is the percentage of nonlinearity (PNL), which quantifies the percentage of modification of the site-response curve between the BSR of each event and the linear site characterization (Régnier et al., 2013). PNL is defined as the ratio of two areas of the site BSR curves within the frequency range of 0.3 to 30 Hz. The first one is the area between the BSR computed from the recording of a given event and the  $\text{BSR}_{\text{linear}}^{95}$  curves, and the second one is the area below the  $\text{BSR}_{\text{linear}}$  curve. The calculation of PNL (in percent) can be expressed as (Régnier et al., 2013):

$$A = \sum_{i=N_1}^{N_2} \begin{cases} (\text{BSR}(i) - \text{BSR}_{\text{linear}}^+(i)) \log_{10}\left(\frac{f_{i+1}}{f_i}\right) & \text{if } \text{BSR}(i) \geq \text{BSR}_{\text{linear}}^+(i) \\ (\text{BSR}_{\text{linear}}^-(i) - \text{BSR}(i)) \log_{10}\left(\frac{f_{i+1}}{f_i}\right) & \text{if } \text{BSR}(i) \leq \text{BSR}_{\text{linear}}^-(i) \\ 0 & \text{otherwise} \end{cases} \quad (2)$$

$$\text{PNL} = \frac{A}{\sum_{i=N_1}^{N_2} |\text{BSR}_{\text{linear}}| \log_{10}\left(\frac{f_{i+1}}{f_i}\right)} \times 100 \quad (3)$$

where  $\text{BSR}_{\text{linear}}^+$  is the upper boundary of  $\text{BSR}_{\text{linear}}^{95}$ ,  $\text{BSR}_{\text{linear}}^-$  is the lower boundary of  $\text{BSR}_{\text{linear}}^{95}$ ,  $f$  is the frequency,  $N_1$  is the first index of the frequency that is above 0.3 Hz, and  $N_2$  is the last index of frequency that is below 30 Hz. Compared to the degree of nonlinearity of site response (DNL) proposed by Wen et al. (2011), PNL takes into account the variability of the linear site-response curve and is normalized by the mean linear site-response curve to give an absolute estimation of the nonlinear behavior of the soil independently of the linear site-response amplitude. In this work, PNL larger than 10% is considered as a nonlinear site response.

##### 3.2.2. Site-specific regression of PNL

PNL values are affected by site conditions and incident motion parameters. Previous studies have shown that PNL correlates well with  $\text{PGA}_{\text{downhole}}$ , an amplitude parameter of incident motion, and this correlation varies from site to site (Régnier et al., 2016). Therefore, it is possible to build site-specific nonlinear regression models for each of the four liquefiable sites to empirically predict PNL given  $\text{PGA}_{\text{downhole}}$  values at these locations. One specific form of the nonlinear regression model is proposed by Régnier et al. (2013) as follows

$$\text{PNL} = a \{ \tanh[\log(\text{PGA}_{\text{downhole}}) - b] + 1 \} \quad (4)$$

where  $a$  and  $b$  are regression coefficients for the specific site. In Section 4, we will perform regression analysis of PNL for the four liquefiable

sites and obtain site-specific regression models.

Furthermore, with the site-specific regression of PNL based on Eq. (4), two nonlinear site parameters are defined to compare the nonlinearity of site responses at different sites. The first nonlinear site parameter, called  $PNL_{site}$ , corresponds to the value of PNL at a threshold value of  $PGA_{downhole}$  (here  $50 \text{ cm/s}^2$ ). The second nonlinear site parameter, called  $PGA_{th}$ , is the threshold value of  $PGA_{downhole}$  at PNL of 10%.  $PGA_{th}$  is the acceleration for which we expect 10% of modification in between linear and nonlinear site responses (Régnier et al., 2013). The sites with higher  $PNL_{site}$  and lower  $PGA_{th}$  values generally have a higher susceptibility to nonlinear site response. The results of  $PNL_{site}$  and  $PGA_{th}$  for the four selected sites will be discussed in Section 4.

### 3.3. Nonlinear event parameter: $fsp$

#### 3.3.1. Definition of $fsp$

The second nonlinear event parameter, termed  $fsp$ , is used to characterize the observed frequency shift of resonance peaks, a characteristic of nonlinear soil behavior (Castro-Cruz et al., 2020). The logarithmic frequency shift is the gap in log-scale between  $BSR_{linear}$  and  $BSR$  of a given event. The algorithm to find this logarithmic shift minimizes the misfit between  $BSR_{linear}$  and  $BSR$  of any given event as (Castro-Cruz et al., 2020):

$$M = \sum_{i=N_3}^{N_4} |BSR_{linear}(\bar{f}/Ls) - BSR(\bar{f})| \log_{10}(f_{i+1}/f_i) \quad (5)$$

$$\bar{f} = \frac{1}{2}(f_{i+1} + f_i) \quad (6)$$

$$fsp = Ls^2 \quad (7)$$

where  $M$  is the misfit and is a discrete approximation of the area between the shifted  $BSR_{linear}$  and  $BSR$ ,  $Ls$  is the logarithmic shift applied to  $BSR_{linear}$ ,  $f$  is the frequency,  $N_3$  is the first index of the frequency that is above 0.3 Hz, and  $N_4$  is the last index of frequency that is below 30 Hz,  $fsp$  is the frequency shift parameter defined as the square of the  $Ls$  that produces the minimum value of  $M$ . Nonlinear soil behavior is expected to shift  $BSR$  to lower frequency range, and therefore, is linked to an  $fsp$  below one (Castro-Cruz et al., 2020).

#### 3.3.2. Site-specific regression of $fsp$

Similar to the site-specific regression analysis of PNL, we will also develop site-specific regression models for  $fsp$  given incident motion parameters. Specifically, a hyperbolic function of the following form (Castro-Cruz et al., 2020) is adopted:

$$fsp = \frac{1}{1 + \frac{PGA_{downhole}}{PGA_{Refdownhole}}} \quad (8)$$

where  $PGA_{Refdownhole}$  is a site-specific parameter defining the hyperbolic function, and it equals to  $PGA_{downhole}$  corresponding to  $fsp$  of 0.5. This formulation is equivalent to the one used to describe the soil shear modulus reduction curves, and  $PGA_{Refdownhole}$  is the counterpart of reference shear strain  $\gamma_{ref}$  in the soil shear modulus reduction. By comparing  $fsp$  values computed from a site with 283 records with the shear modulus reduction curves obtained from cyclic triaxial tests, Castro-Cruz et al. (2020) observed that the  $fsp$  values are in the range of the shear modulus reduction curves, and therefore,  $fsp$  is a good proxy for the shear modulus reduction with shear strain.

In this study, we interpret  $PGA_{Refdownhole}$  as the third nonlinear site parameter (in addition to  $PNL_{site}$  and  $PGA_{th}$ ) describing the site's susceptibility to nonlinear site response. Different from  $PGA_{th}$  that indicates the 10% modification to linear site response,  $PGA_{Refdownhole}$  is interpreted as the threshold  $PGA_{downhole}$  value beyond which a significant nonlinear site response might be expected. This indicates that sites with lower  $PGA_{Refdownhole}$  values are more susceptible to nonlinear site

response.

It is worth noting that the recordings of liquefaction-triggering events are excluded when performing the regression analyses as liquefaction-triggering events are rare events for the four selected vertical arrays due to the short instrumentation period. More importantly, we will separate these liquefaction-triggering events to test if the regression models derived from general site responses (i.e., responses with non-liquefied status) can successfully predict the site response affected by liquefaction. Such an approach allows us to test the hypothesis that liquefaction could deviate the site response from both common linear and nonlinear site responses. Details of the analyses will be presented in Section 4.

## 4. Results and analyses

With the vertical array data compiled in Section 2 and the methodology described in Section 3, in this section, we present the analysis results of the four vertical arrays and show how liquefaction could significantly modify the site response from the common linear and nonlinear site responses. For each site, we present first the site response  $BSR$  curves computed from all ground motions and discuss the modifications of liquefaction on site response. Then, we develop site-specific empirical regression models for the two nonlinear event parameters (PNL and  $fsp$ ) and discuss the deviation of the liquefaction-affected parameters from regression models.

### 4.1. Wildlife Liquefaction Array

**Fig. 5a** shows the  $BSR$  curves computed from all ground motions at the WLA site with a gray intensity corresponding to the  $PGA_{downhole}$  value. The site response curves are strongly modified as  $PGA_{downhole}$  changes. The site response curves of the liquefaction-triggering event (the 1987  $M_w$  6.6 Superstition Hills event with a  $PGA_{downhole}$  of  $175.5 \text{ cm/s}^2$ ) and the two events generating nonlinear soil behavior (the  $M_w$  4.9 and  $M_w$  4.6 events from the 2012 Brawley swarm with a  $PGA_{downhole}$  of  $277.1$  and  $220.2 \text{ cm/s}^2$ , respectively) are shown in **Fig. 5b** along with the mean and 95% confidence intervals of the linear site response  $BSR$  curves. The two nonlinear site responses show the typical nonlinear site response characteristics, i.e., the resonance frequency shift and the decrease of  $BSR$  amplitude compared to  $BSR_{linear}$ . In addition, the 2012  $M_w$  4.9 event (the solid black curve in **Fig. 5b**) slightly modifies the shape of the site response curve, where there are two flat regions, one at the frequency range of  $2 \sim 3 \text{ Hz}$  and one at  $10 \sim 15 \text{ Hz}$ .

Moreover, **Fig. 5b** shows that soil liquefaction induces significantly different site responses compared to the two nonlinear events. The site response curve of the liquefaction-triggering event (the red curve in **Fig. 5b**) is significantly different from the nonlinear curves, which indicates liquefaction can drastically change the shape of the site response curve and induce irregular amplification modes. For this liquefaction triggering event, the maximum pore water pressure ratio is 1.0, and liquefaction significantly amplifies the low-frequency ground motion components (at the frequency range of  $0.2 \sim 2.0 \text{ Hz}$ ), where the peak  $BSR$  is reached at the frequency of around 0.25 Hz. Simultaneously, liquefaction de-amplifies  $BSR$  in the  $2 \sim 8 \text{ Hz}$  frequency part. Although these observations are site-specific, they provide direct evidence that pore water pressure generation and liquefaction could lead to very different site responses from common linear and nonlinear ones.

The relationships between the two nonlinear event parameters (PNL and  $fsp$ ) with the incident-motion parameter ( $PGA_{downhole}$ ) are shown in **Fig. 6**. It can be seen that PNL and  $fsp$  correlate well with  $PGA_{downhole}$  at the WLA site. Coefficients of the site-specific regression models fitted using Eq. (4) for PNL and Eq. (8) for  $fsp$  and the nonlinear site parameters derived from the regression models are summarized in **Table 3**. It is noted the value of  $fsp$  corresponding to the liquefaction-triggering event is higher than the trend line predicted using other events (see **Fig. 6b**). The calculation of  $fsp$  is based on the assumption that the nonlinear site

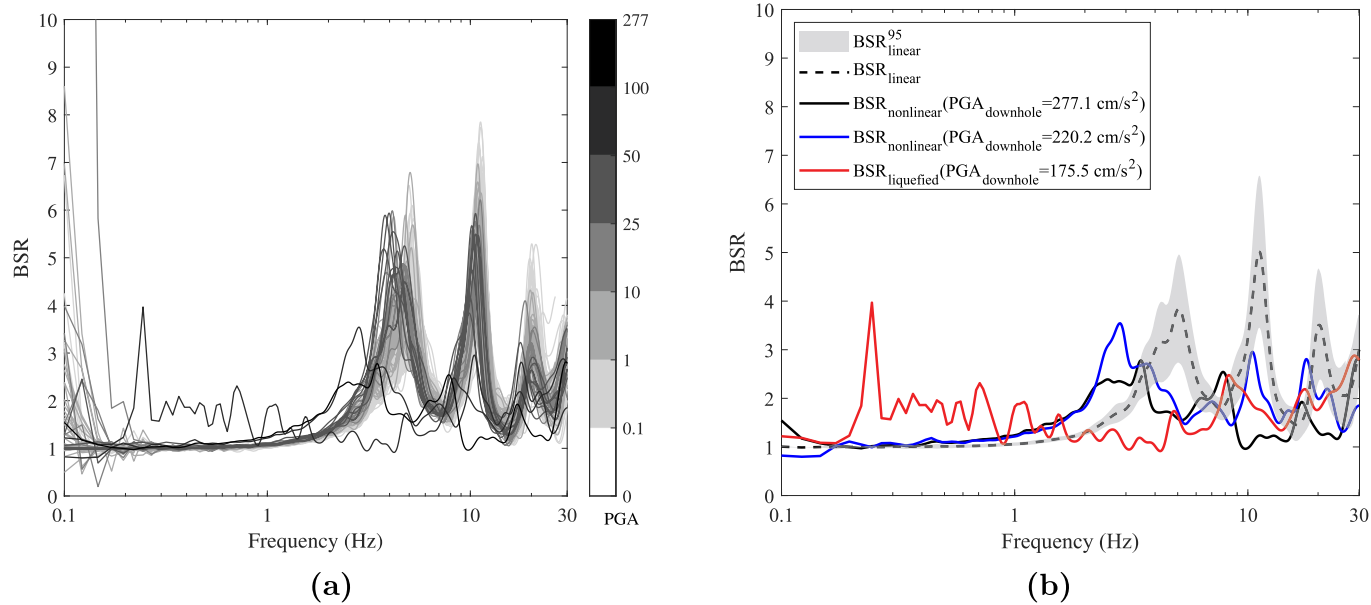


**Fig. 5.** (a) BSR curves at the WLA site computed from all ground motions. (b) BSR curves under different site response states. Black dashed line and gray area represent the mean values and 95% confidence interval of borehole spectra ratios computed from weak motions only, respectively. The black, blue, and red solid lines are for the M<sub>w</sub> 4.9 and M<sub>w</sub> 4.6 swarm events, and the M<sub>w</sub> 6.6 Superstition Hills earthquake, respectively. (For interpretation of the references to colour in this figure legend, the reader is referred to the web version of this article.)

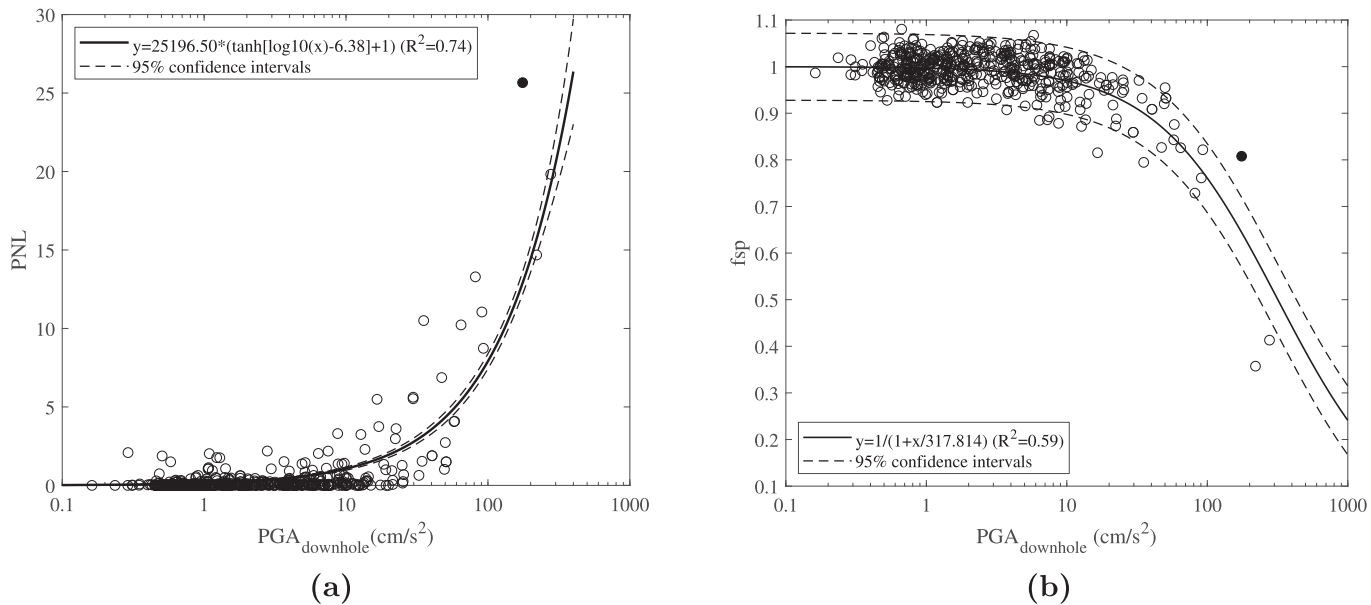


**Fig. 6.** PNL and fsp values versus PGA<sub>downhole</sub> for the WLA site. The filled circle is from the 1987 Superstition Hills earthquake that triggered liquefaction.

**Table 3**

Regression relationships between PNL, fsp and downhole PGA, and nonlinear site parameters for each site.

Station	$PNL = a \{ \tanh[\log(PGA_{downhole}) - b] + 1 \}$			PNL <sub>site</sub>	PGA <sub>th</sub>	f <sub>SP</sub> = $\frac{1}{1 + \frac{PGA_{downhole}}{PGA_{Refdownhole}}}$	R <sup>2</sup>
	a	b	R <sup>2</sup>				
Wildlife	25,196.50	6.38	0.74	4.3	133.9	317.8	0.59
Port Island	2395.42	5.38	0.43	3.2	245.3	325.3	0.5
Kushiro Port	8.57	1.82	0.44	7.5	97.4	260.2	0.8
Onahama Port	3.96	1.75	0.18	3.8	-	275.9	0.23

response does not change the shape of the site response curve while only shifts the resonance peaks towards lower frequencies (Castro-Cruz et al., 2020). Hence, it is impractical to use  $f_{sp}$  and linear site response curves to predict the site response for events where liquefaction may take effect since liquefaction can significantly change the shape of the site response curve.

#### 4.2. Port Island Array

The 1995 M<sub>JMA</sub> 7.3 Hyogoken-Nanbu earthquake triggered liquefaction at the PIA site, and the sand ejecta continued one hour after the mainshock (Yamazaki et al., 1995). Here, we denote the ground motion of this mainshock as liquefied (with a PGA<sub>downhole</sub> of 723.2 cm/s<sup>2</sup>) and its M<sub>JMA</sub> 5.0 aftershock (occurred 7 min after the mainshock and with a PGA<sub>downhole</sub> of 165.6 cm/s<sup>2</sup>) as post-liquefied. Fig. 7a shows the site response BSR curves computed from all ground motions at the PIA site with a gray intensity corresponding to the PGA<sub>downhole</sub> value, and Fig. 7b shows the site response curves of the liquefied, the post-liquefied, and a nonlinear event along with the mean and 95% confidence intervals of the linear site response curves. Soil liquefaction and post-liquefied states induced significantly different site responses compared to other events. For the PIA site, the event with the third-largest PGA<sub>downhole</sub> value (i.e., 66.3 cm/s<sup>2</sup>) did not trigger nonlinear site response, as its BSR curve (the black solid curve in Fig. 7b) is very similar to the linear BSR curves.

For the liquefaction-triggering event (the red curve in Fig. 7b), the site response is significantly amplified at the low-frequency range (0.1–0.25 Hz), and the peak BSR is reached at 0.12 Hz. Simultaneously, liquefaction de-amplifies the site response for frequencies larger than 0.7 Hz. For the post-liquefaction event (the blue curve in Fig. 7b), the site response is de-amplified for frequencies exceeding 1.5 Hz and amplified at two relatively low-frequency ranges (0.25–0.8 Hz, and 1.2–1.5 Hz). The peak BSR frequency of the post-liquefied event is the same as the linear site response, while the peak BSR value reaches the upper limit of linear site response. These findings suggest that liquefaction can de-amplify the high-frequency ground motions while amplifies the low-frequency ranges. Meanwhile, the de-amplification at the high-frequency range is preserved for the post-liquefied major aftershock that occurred seven minutes after the mainshock. It implies the

site-specific drainage conditions may influence the liquefaction duration as well as the site response stage.

The relationships between the two nonlinear event parameters (PNL and  $f_{sp}$ ) with PGA<sub>downhole</sub> are shown in Fig. 8. Coefficients of the regression models (Eq. (4) and Eq. (8)), as well as the nonlinear site parameters (PNL<sub>site</sub> and PGA<sub>th</sub>) derived from the regression models, are summarized in Table 3. Although the coefficients of determination ( $R^2$ ) value of the regression models are relatively low at the PIA site, there is a trend that the  $f_{sp}$  and PNL are correlated with PGA<sub>downhole</sub> as shown in Fig. 8. It is noted that the regression models are not well constrained due to the lack of strong-motion observations at the PIA site. For the liquefaction-triggering and the post-liquefaction event (the 1995 M<sub>JMA</sub> 7.3 Hyogoken-Nanbu mainshock and its major aftershock), the PNL values are significantly higher while the  $f_{sp}$  values are much lower than those of the other events, indicating that liquefaction can induce a high degree of nonlinearity in site responses.

#### 4.3. Kushiro Port Array

As described in Section 2, there were three earthquakes that had triggered liquefaction at the KPA site, i.e., the 1993 M<sub>JMA</sub> 7.5 Kushiro-Oki earthquake (PGA<sub>downhole</sub>=276.9 cm/s<sup>2</sup>), the 2003 M<sub>JMA</sub> 8 Tokachi-Oki earthquake (PGA<sub>downhole</sub>=229.5 cm/s<sup>2</sup>), and the 1994 M<sub>JMA</sub> 8.2 Hokkaido Toho-Oki earthquake (PGA<sub>downhole</sub>=115.6 cm/s<sup>2</sup>). Fig. 9a shows the BSR curves computed from all ground motions at the KPA site with a gray intensity corresponding to the PGA<sub>downhole</sub> value. The site response curves of the three liquefaction-triggering events and an event generating nonlinear soil behavior (the 2004 off-Kushiro earthquake with a PGA<sub>downhole</sub> of 136.7 cm/s<sup>2</sup>) are shown in Fig. 9b along with the mean and 95% confidence intervals of the linear site response BSR curves.

For the KPA site, the inter-event variability of the linear site responses is relatively large, especially for frequencies exceeding 10 Hz, which likely reflects the high lateral heterogeneity of the subsurface soil. In other words, the assumption of 1D profile for the linear site response analysis may not hold for the KPA site, and therefore, the incident angle of ground motions can change the site response (personnel communication with Julie Régnier).

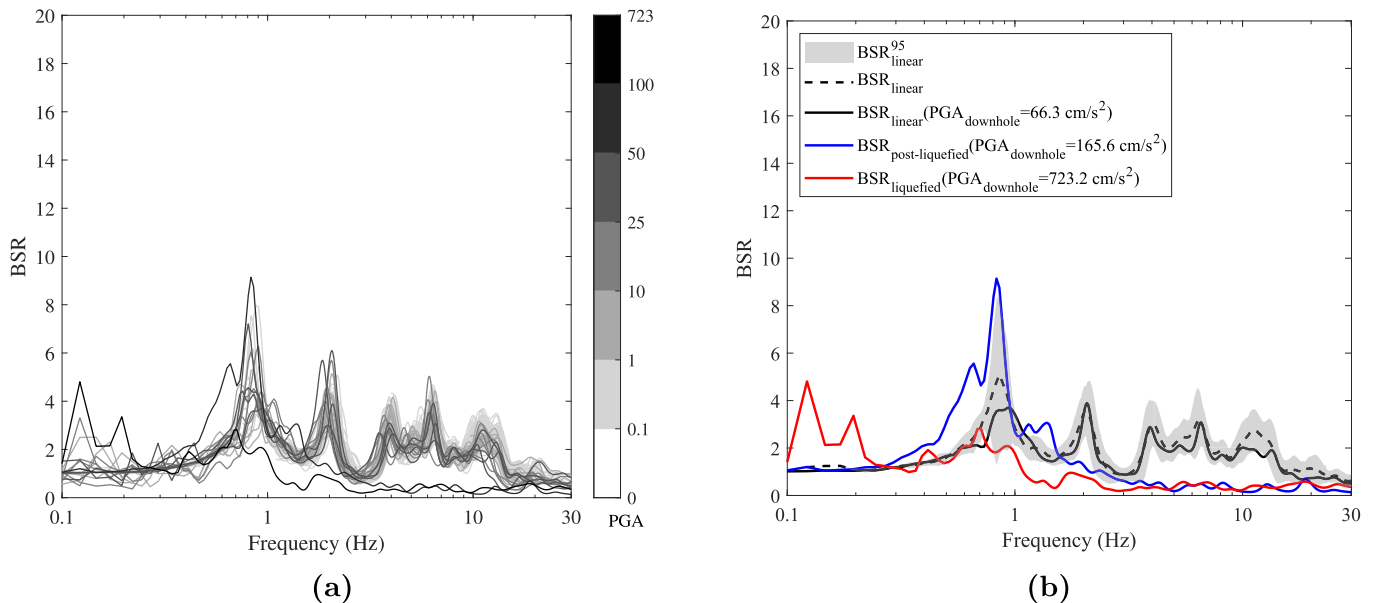


**Fig. 7.** (a) BSR curves at the PIA site computed from all ground motions. (b) BSR curves under different site response states. Black dashed line and gray area represent the mean values and 95% confidence interval of borehole spectra ratios computed from weak motions only, respectively. The red, blue, and black solid lines are for the 1995 M<sub>JMA</sub> 7.3 Hyogoken-Nanbu earthquake, its major aftershock, and the 2013 M<sub>JMA</sub> 6.3 earthquake, respectively. (For interpretation of the references to colour in this figure legend, the reader is referred to the web version of this article.)

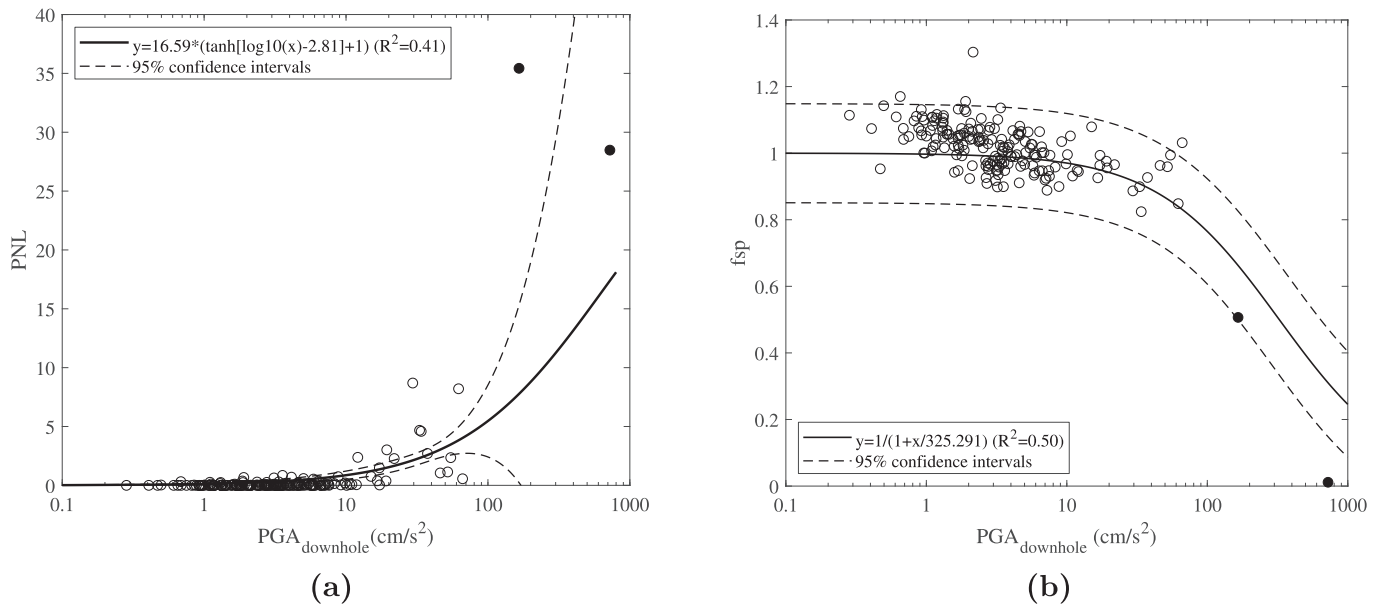


**Fig. 8.** PNL and  $f_{sp}$  values versus  $\text{PGA}_{\text{downhole}}$  for the PIA site. The filled circles from the right to left are the mainshock of the 1995  $M_{\text{JMA}} 7.3$  Hyogoken-Nanbu, and the major aftershock occurred 7 min after the mainshock.

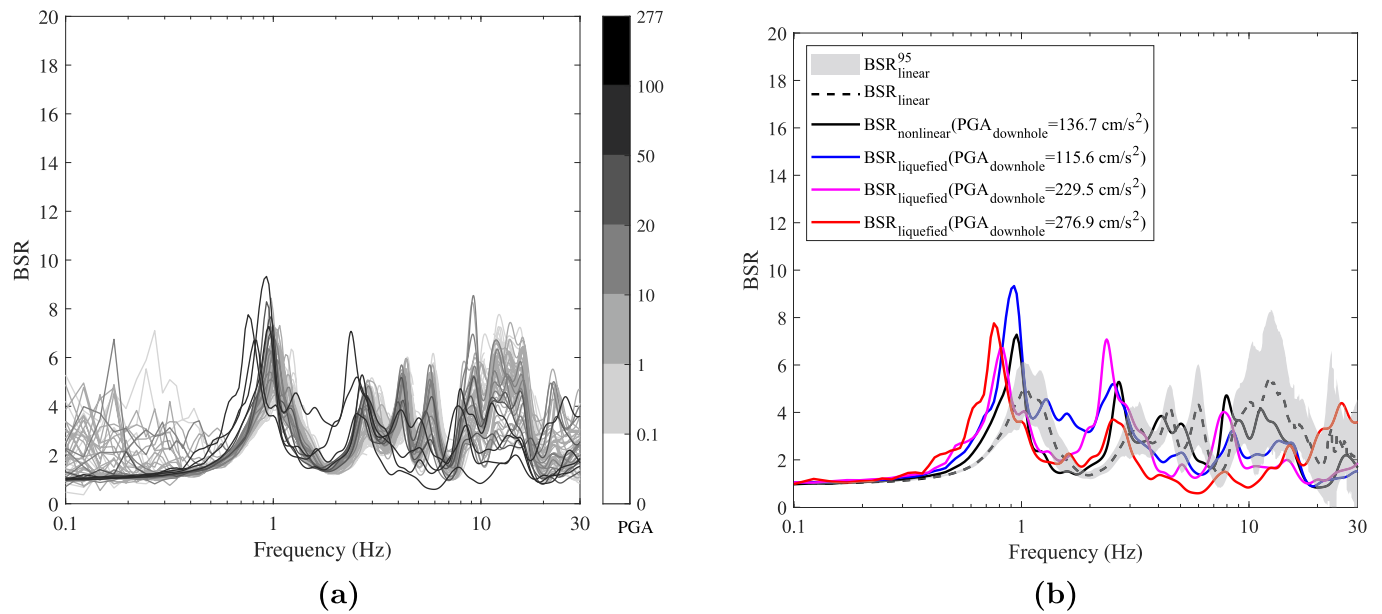


**Fig. 9.** (a) BSR curves at the KPA site computed from all ground motions. (b) BSR curves under different site response states. Black dashed line and gray area represent the mean values and 95% confidence interval of borehole spectra ratios computed from weak motions only, respectively. The red, magenta, blue, and black solid lines are for the 1993  $M_{\text{JMA}} 7.5$  Kushiro-Oki earthquake, the 2003  $M_{\text{JMA}} 8.0$  Tokachi-oki earthquake, the 1994  $M_{\text{JMA}} 8.2$  Hokkaido Toho-Oki earthquake, and the 2004  $M_{\text{JMA}} 7.1$  off-Kushiro earthquake, respectively. (For interpretation of the references to colour in this figure legend, the reader is referred to the web version of this article.)

Despite this high variability, liquefaction-triggering events show distinct site responses compared to both common nonlinear and linear site responses. The nonlinear site response curve of the 2004 off-Kushiro earthquake (the solid black curve in Fig. 9b) shifts the linear site response to lower frequencies and increases the peak BSR at two lower frequencies (0.9 and 2.8 Hz). The liquefaction-triggering events not only shift the peak BSR to lower frequencies but also change the shape of the site response curve. The site response of the 1993 Kushiro-Oki earthquake de-amplifies the ground motion with frequencies between 3 and 20 Hz, while slightly amplifies the ground motions with frequencies exceeding 20 Hz. Both the 1994 Hokkaido Toho-Oki earthquake and the

2003 Tokachi-Oki earthquake de-amplify the ground motions with frequencies exceeding 3 Hz. While the 1994 event strongly amplifies the ground motions with frequencies close to 0.9 Hz, and the 2003 event strongly amplifies the ground motions with frequencies close to 2.5 Hz.

The relationships between the two nonlinear event parameters (PNL and  $f_{sp}$ ) with  $\text{PGA}_{\text{downhole}}$  are shown in Fig. 10. We observe that  $f_{sp}$  and PNL correlate relatively well with  $\text{PGA}_{\text{downhole}}$ . The coefficients of regression models (Eqs. (4) and (8)), as well as the nonlinear site parameters derived from the regression models, are listed in Table 3. For the three liquefaction-triggering events, the PNL values are significantly higher while the  $f_{sp}$  values are much lower than those of the other

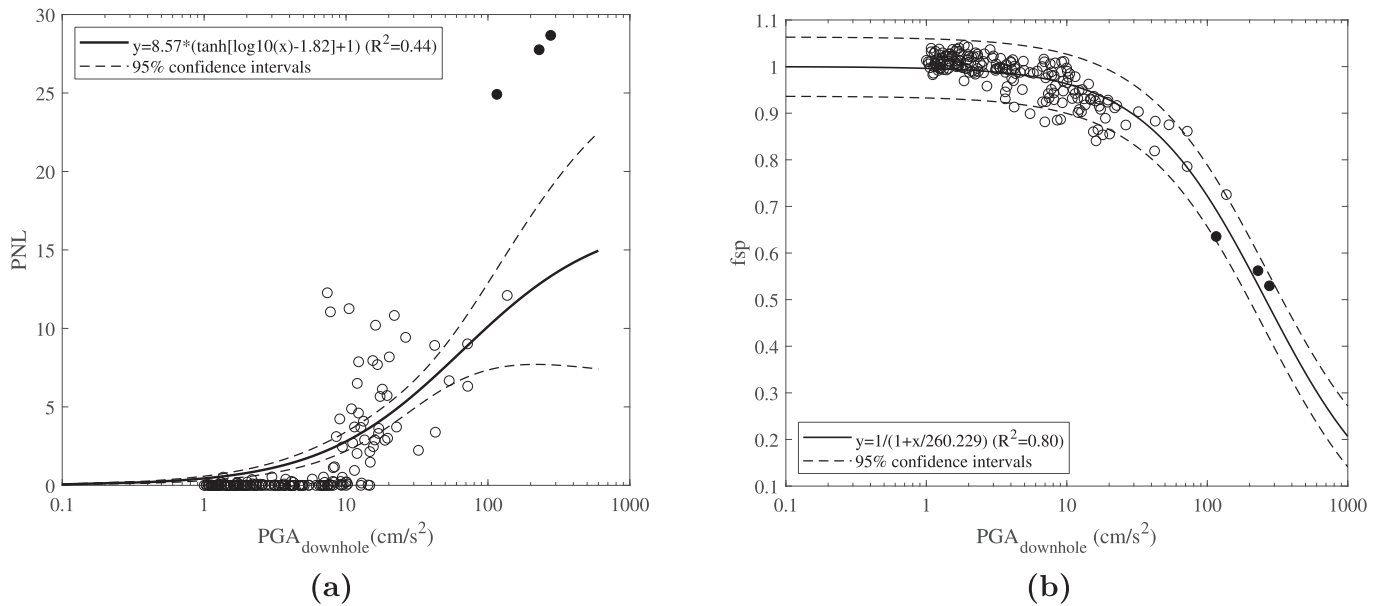


**Fig. 10.** (a) PNL and  $f_{sp}$  values versus  $\text{PGA}_{\text{downhole}}$  for the KPA site. The filled circle from right to left are from the 1993  $M_{\text{JMA}} 7.5$  Kushiro-Oki, the 2003  $M_{\text{JMA}} 8$  Tokachi-Oki, and the 1994  $M_{\text{JMA}} 8.2$  Hokkaido Toho-Oki earthquakes that induced liquefaction.

events, indicating that liquefaction induced a high degree of nonlinearity in site responses.

#### 4.4. Onahama Port Array

Fig. 11a shows the site response BSR curves computed from all ground motions at the OPA site with a gray intensity corresponding to the  $\text{PGA}_{\text{downhole}}$  value. The site response curves of the liquefaction-triggering event (the 2011  $M_{\text{JMA}} 9.0$  Tohoku earthquake with a  $\text{PGA}_{\text{downhole}}$  of  $196.8 \text{ cm/s}^2$ ) and two events generating nonlinear (non-liquefied) soil behavior (corresponding to the 2013  $M_{\text{JMA}} 5.9$  Eastern Honshu earthquake and the 2016  $M_{\text{JMA}} 7.4$  Fukushima earthquake, with a  $\text{PGA}_{\text{downhole}}$  of  $131.8 \text{ cm/s}^2$  and  $106.2 \text{ cm/s}^2$ , respectively) are shown

in Fig. 11b along with the mean and 95% confidence intervals of the linear site response curves. The two nonlinear site responses (the black and blue solid curves in Fig. 11b) show the characteristics of predominant frequency shift and the decrease in BSR amplitude compared to  $\text{BSR}_{\text{linear}}$ . In addition, the 2016  $M_{\text{JMA}} 7.4$  Fukushima earthquake (the blue solid line on Fig. 11b) generated a larger frequency shift than the 2013  $M_{\text{JMA}} 5.9$  Eastern Honshu event (the black solid line in Fig. 11b), although the 2016 event has a lower value of  $\text{PGA}_{\text{downhole}}$ , indicating the need for additional parameters to quantify the nonlinear site response.

The site response curve of the liquefaction-triggering event (the red solid line in Fig. 11b) is significantly different from those of the other events. Liquefaction significantly amplifies the low-frequency ground motion components (frequency range of  $0.8 \sim 4.0 \text{ Hz}$ ), and de-amplifies

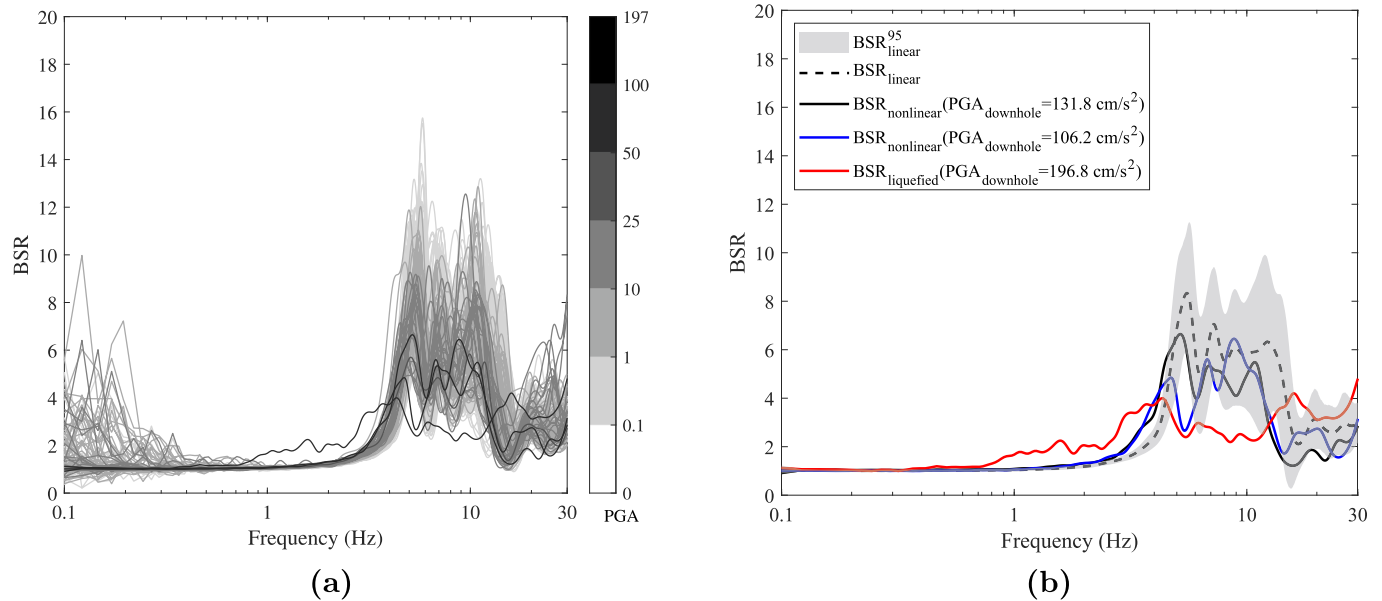


**Fig. 11.** (a) BSR curves at the PIA site computed from all ground motions. (b) BSR curves under different site response states. Black dashed line and gray area represent the mean values and 95% confidence interval of borehole spectra ratios computed from weak motions only, respectively. The red, blue, and black solid lines are for the 2011  $M_{\text{JMA}} 9.0$  Tohoku earthquake, the 2016  $M_{\text{JMA}} 7.4$  Fukushima earthquake, and the 2013  $M_{\text{JMA}} 5.9$  Eastern Honshu earthquake, respectively. (For interpretation of the references to colour in this figure legend, the reader is referred to the web version of this article.)

the middle-frequency apart (frequency range of 4.0 ~ 15.0 Hz). Moreover, this event amplifies the site response for frequencies exceeding 15.0 Hz, and the peak BSR occurred at a frequency larger than 30 Hz. This high-frequency amplification is related to several dilation-induced acceleration pulses (Roten et al., 2013). One possible cause is that the pore water pressure dissipated easily because of good drainage conditions, and the site had never become extremely soft at any point during the record (Kramer et al., 2016).

The relationships between the two nonlinear event parameters (PNL and *fsp*) with PGA<sub>downhole</sub> are shown in Fig. 12. Similar to the other sites, both *fsp* and PNL correlate well with PGA<sub>downhole</sub>. The coefficients of the site-specific regression models (Eq. (4) and Eq. (8)) and the nonlinear site parameters derived from the regression models are summarized in Table 3. It is noted that R<sup>2</sup> values for both regression models are relatively low, and the PNL values of some weak events are unexpectedly high (shown in Fig. 12a), which indicates large variability of linear site responses at the OPA site. Due to such a large variability, PGA<sub>th</sub> cannot be obtained at the OPA site as the PNL regression model is not well constrained (see Fig. 12a). Fig. 12b shows the *fsp* value gradually decreases with PGA<sub>downhole</sub>, which is as expected as the site is composed mostly of stiff soils that require stronger shaking intensity to soften the soil structure. The PGA<sub>th</sub> of OPA is unobtainable as the PNL value estimated using PGA<sub>downhole</sub> cannot reach 10 (namely, 10% modification to the linear site response curve).

## 5. Discussion

### 5.1. Variability in liquefied site responses

In Section 4, we analyzed the effects of liquefaction on nonlinear site response at the four liquefiable sites, which are site-specific and event-specific. In this section, we aim to discuss the observed variability across the four sites and the possible causes using available site information. To compare the site responses under different liquefaction-triggering events at different sites, we calculate the nonlinear to linear site-response ratio (R<sub>NL-L</sub>) defined as the ratios between the borehole spectral ratios for liquefaction-triggering events and the mean borehole spectral ratios (BSR<sub>linear</sub>) for weak events. The R<sub>NL-L</sub> curves of the selected liquefaction-triggering events at the four liquefiable sites are shown in Fig. 13.

From Fig. 13, we observe that liquefaction tends to amplify low- and

very-high-frequency ground motions while de-amplifying medium-frequency ground motions when compared to the linear site response. Peak R<sub>NL-L</sub> values occur at very low frequencies at the WLA and PIA sites (0.25 and 0.15 Hz, respectively), with the peak value reaching 4. Peak R<sub>NL-L</sub> values reach 3 and 2 at 0.85 Hz and 3 Hz for the KPA and OPA sites, respectively. Liquefaction only amplifies the very-high-frequency ground motions at KPA and OPA, with the peak R<sub>NL-L</sub> values reaching about 2 at 20 Hz and 15 Hz, respectively. Even though the peak R<sub>NL-L</sub> values at very high frequencies are relatively low, i.e., close to 2 for the KPA and OPA sites, the liquefaction-induced high-frequency amplification could still significantly affect the surface PGA when the incident motions are also rich in high-frequency motions. Taking the 2011 M<sub>JMA</sub> 9.0 Tohoku earthquake recordings at the OPA as an example, PGA<sub>surface</sub> is nine times higher than PGA<sub>downhole</sub> (see Table 2). This strong amplification of surface PGA is linked to both the site response (liquefaction and pore water pressure activity) and earthquake source characteristics (a burst of high-frequency motions from a large slip patch) (Roten et al., 2013). The minimum R<sub>NL-L</sub> values reach about 0.1 to 0.3, which suggests a strong de-amplification at medium frequencies.

We suggest it is the site-specific characteristics of liquefiable soil that play an important role in the observed variability of nonlinear site response at liquefiable sites. As described in Section 2, the liquefiable soil layers of the WLA and PIA are loose sandy soils with an average SPT N-value of about 7, while the liquefiable soil layers of the KPA and OPA are dense soils with an average SPT N-value above 20. These two types of soils may have different liquefaction mechanisms under strong motions. Loose soils may undergo flow liquefaction in which the soil can be very soft once the liquefaction initiation occurs. The dilatancy behavior of dense sands can produce the partial recovery of the soil strength under cyclic loads, which translates into the ability to produce large deformations followed by large and spiky shear stresses (Bonilla et al., 2005; Roten et al., 2013).

### 5.2. Empirical *fsp* model for predicting site responses

The nonlinear event parameter *fsp* has been adopted in this work to quantify the observed frequency shift of resonance peaks, which is characteristic of nonlinear site response. According to Castro-Cruz et al. (2020), *fsp* can be used to not only quantify the nonlinearity in site response but also predict nonlinear site responses and surface ground motions. The approach consists of first applying the predicted frequency

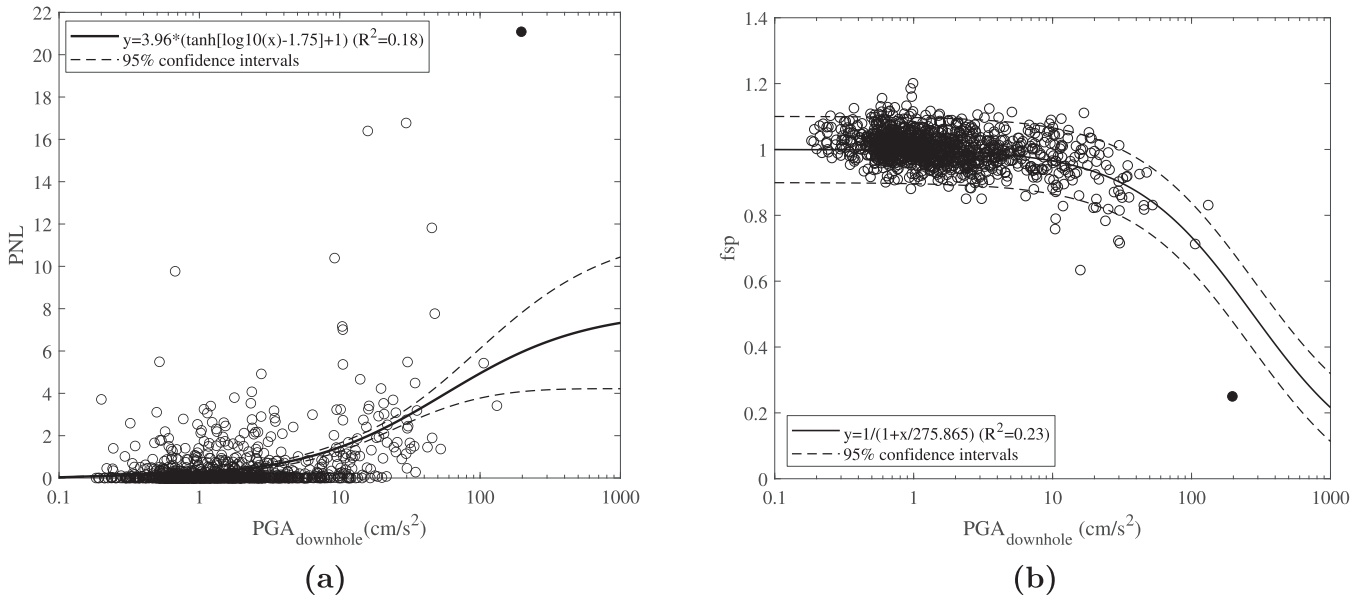


**Fig. 12.** PNL and *fsp* values versus PGA<sub>downhole</sub> for the OPA site. The filled circle is from the 2011 M<sub>JMA</sub> 9.0 Tohoku earthquake that triggered liquefaction.

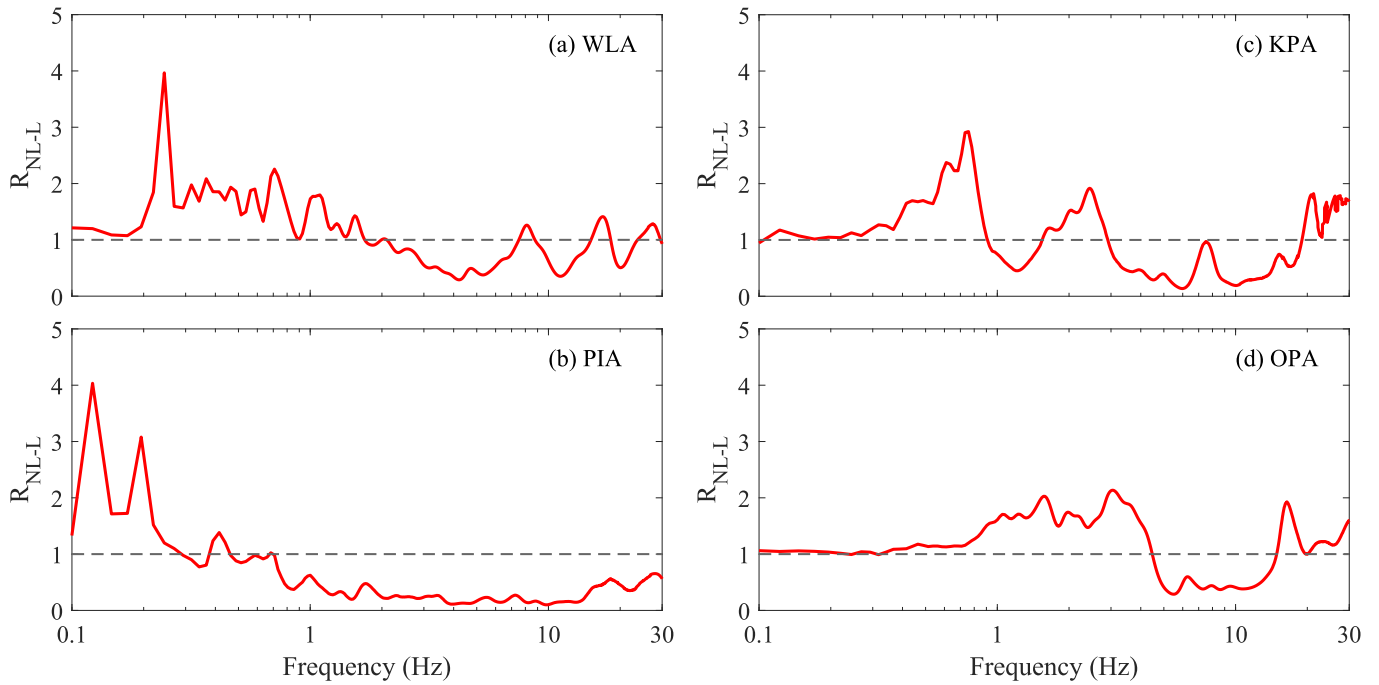


**Fig. 13.** Nonlinear to linear site-response ratio curves for the liquefaction-triggering events at the four vertical arrays. (a) the 1987  $M_w$  6.6 Superstition Hills earthquake at the WLA; (b) the 1995  $M_{JMA}$  7.3 Hyogoken-Nanbu earthquake at the PIA; (c) the 1993  $M_{JMA}$  7.5 Kushiro-Oki earthquake at the KPA; and (d) the 2011  $M_{JMA}$  9.0 Tohoku earthquake at the OPA. The event information are as same as ones in the BSR curves for each array.

shift as

$$\widehat{BSR}(f) = BSR_{\text{linear}}(f \cdot \sqrt{fsp}) \quad (9)$$

where  $\widehat{BSR}$  is the estimated nonlinear borehole spectral ratio corresponding to a strong motion,  $BSR_{\text{linear}}$  is the linear bore spectral ratio,  $fsp$  is the estimated frequency shift from the site-specific hyperbolic curve (Eq. (8)),  $f$  is the frequencies. Then, the surface ground motion is estimated using

$$\widehat{FAS}_{\text{surface}} = \widehat{BSR}(f) \cdot FAS_{\text{downhole}} \quad (10)$$

where  $FAS_{\text{downhole}}$  is the Fourier amplitude spectrum of horizontal components of the recorded downhole ground motion, and  $\widehat{FAS}$  is the estimated Fourier amplitude spectrum of horizontal components of the surface ground motions. The estimated site response (i.e.,  $BSR(f)$ ) can be used as an empirical transfer function to convert the Fourier amplitude spectrum of downhole recordings to the Fourier amplitude spectrum of surface recordings (through Eq. (10)). Castro-Cruz et al. (2020) have shown a successful application of this approach to the 2016  $M_w$  7.1 Kumamoto earthquake in Japan.

A key underlying assumption of the above approach is that the nonlinear soil behavior only shifts the resonance peaks towards lower frequencies, and the shape of the BSR curves is preserved. For liquefiable sites, however, the shapes of BSR curves under liquefaction-triggering conditions are significantly modified compared to the linear BSR curves (e.g., Figs. 5b, 7b, 9b, and 11b), which may invalidate the above approach when applied to liquefaction-triggering events. Given the significant deviation of the liquefied site response from typical linear and nonlinear site responses observed in this work, we suggest that the BSR curves for liquefied events in Figs. 5b, 7b, 9, and 11b be used as empirical transfer functions to predict liquefied site response for the four sites analyzed in this work. For other liquefiable sites that have similar properties to the four sites investigated in this work, engineers and seismologists may modify the linear site response calibrate by weak

motion observations or numerical simulations following the trends illustrated in Figs. 5b, 7b, 9b, and 11b. In addition, the site-specific regression results in Table 3 may be used to guide the selection of threshold excitation ground motion intensities for different levels of nonlinear site response. However, these results should be applied with caution because seismic site response at liquefiable sites can be influenced by various site conditions (e.g., thickness of a liquefied layer, strata) and earthquake source conditions (e.g., input motion, azimuth) (Kishida and Tsai, 2021; Ko and Chen, 2020; Tsai et al., 2020).

The resonance frequency shift observed in the BSR curves is usually interpreted as a direct effect of shear modulus reduction of the soils, and the decrease in BSR amplitude is interpreted as an effect associated with the increase of soil damping (Castro-Cruz et al., 2020). The strong deviation of BSR curve under liquefaction-triggering conditions could be induced by the more complex nonlinear behavior of soil liquefaction (e.g., phase change, pore water generation and dissipation) (Bonilla et al., 2005). Further studies should be conducted to investigate the mechanism of liquefaction effects on site responses and explore the applicability of empirical methods in predicting the liquefied site responses from linear site responses.

## 6. Conclusions

In this work, we have analyzed the nonlinear site responses at liquefiable sites using more than 2000 ground motion observations at four high-quality downhole arrays that have liquefied during at least one earthquake, including Wildlife Liquefaction Array (WLA), Port Island Array (PIA), Kushiro Port Array (KPA), Onahama Port Array (OPA). The borehole spectral ratio (BSR) curves, computed as the ratio between the geometric average of the Fourier amplitude spectra of the horizontal ground motion components recorded at the surface and at downhole, are used to characterize the frequency-dependent site amplification. Two nonlinear event parameters, the percentage of nonlinearity (PNL) and the frequency shift parameter ( $fsp$ ), are used to quantify the modification of site response of strong events to that of weak events. Then, site-

specific regression analyses have been performed to empirically predict PNL and *fsp* using downhole PGA site-specific regression coefficients. Two PGA threshold values,  $\text{PGA}_{\text{th}}$  and  $\text{PGA}_{\text{Refdownhole}}$ , are derived from the site-specific regression analyses to evaluate the susceptibility of a site to nonlinear site response. Main findings from this study include:

1. The raw BSR curves suggest the liquefaction occurrence could lead to a significant deviation of site responses from common linear and nonlinear site responses at all four examined sites. Liquefaction can not only shift the resonance frequency to lower frequency, but also modify the broadband amplification modes.
2. Liquefaction can enhance the amplification of low-frequency and very-high-frequency ground motions. When compared to linear site responses, the liquefied site responses may be amplified up to 2 to 4 times at low frequencies and up to 2 times at very high frequencies, while they may be de-amplified to 0.1 to 0.3 times at medium frequencies.
3. PNL and *fsp* can characterize the modification of nonlinear soil behaviors on site response. All liquefaction-triggering events yielded PNL values larger than 20, which suggests at least a 20% derivation from the mean linear site amplification curve. The frequency shift parameter (*fsp*) of liquefaction-triggering events ranges from 0.01 to 0.8, with an average value of 0.47. As *fsp* is a good proxy for shear modulus reduction (Castro-Cruz et al., 2020), this finding implies that the soil shear modulus of the entire soil column between two accelerometers (with thickness ranging from 7.7 to 83 m) may be reduced by about 47% on average under liquefaction-triggering conditions.
4. Site-specific univariate regression models were developed to predict PNL and *fsp* at the four selected sites given input downhole PGAs. Preliminary results of this study suggest that PNL and *fsp* are strongly correlated with downhole PGAs, but the predictive accuracy of univariate regression models could be influenced by other factors.

Results of this study provide strong evidence that site responses at liquefiable sites are complex, and could vary from linear to nonlinear, and to liquefied status. Based on the extensive analysis presented in this work, the current site response methods (e.g., linear, equivalent-linear, and total stress nonlinear methods) would be inadequate when they are applied to predict the liquefied response. As strong ground motions at liquefiable sites may remain limited, especially in the low-seismic-risk region, future work will continue data collection and empirical analysis and will employ advanced numerical models to investigate the site response characteristics at liquefiable sites.

## Data and resources

Acceleration time histories and soil profiles of Wildlife Liquefaction Array used in this study were collected from the NEES@UCSB website <http://nees.ucsb.edu/facilities/wla>; Acceleration time histories and soil profiles of the Port Island, Kushiro Port, and Onahama Port Arrays were collected from the PARI website <https://www.pari.go.jp/> (last accessed May 2020).

## CRediT authorship contribution statement

**Weiwei Zhan:** Conceptualization, Methodology, Software, Writing – original draft. **Qiushi Chen:** Conceptualization, Writing – review & editing, Supervision, Funding acquisition.

## Declaration of Competing Interest

The authors declare that they have no known competing financial interests or personal relationships that could have appeared to influence the work reported in this paper.

## Acknowledgments

The authors are indebted to Dr. Julie Régnier who gave valuable advice on empirical site response analysis using borehole spectral ratios. The authors would also like to thank Prof. Yosuke Nagasaka and Prof. Jamison Steidl for providing data of the three Japanese stations and the Wildlife Liquefaction Array, respectively.

## Appendix A. Earthquake information

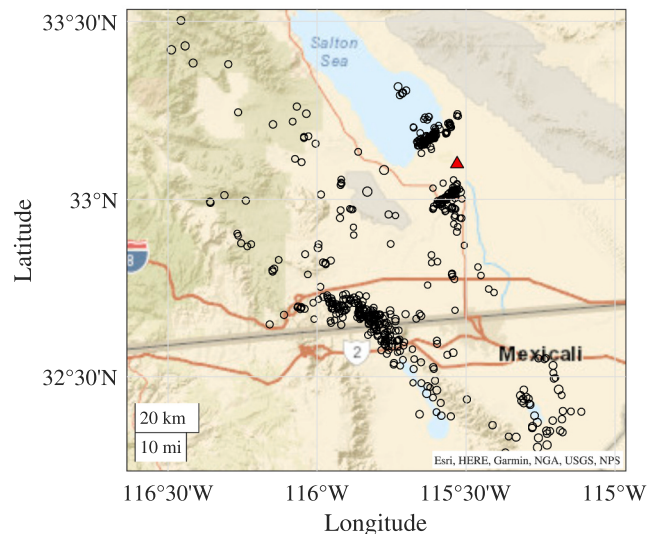


**Fig. A1.** Earthquake epicenter map of events recorded at the WLA site. The red triangle indicates the location of the WLA site. (For interpretation of the references to colour in this figure legend, the reader is referred to the web version of this article.)

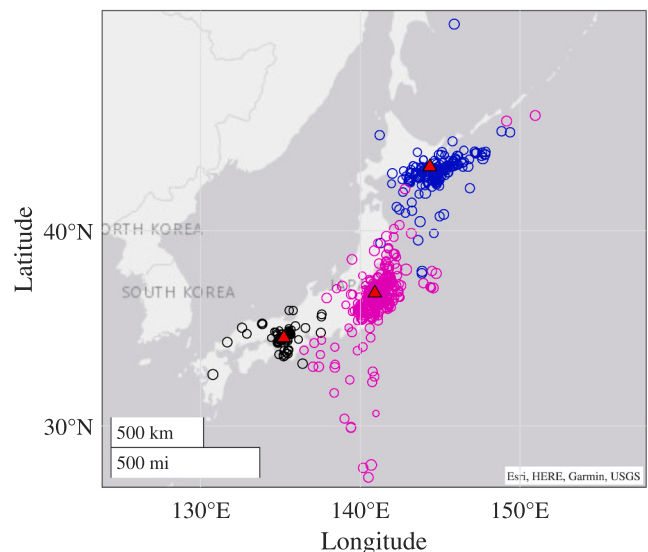


**Fig. A2.** Earthquake epicenter map of events recorded at three Japanese sites. The black, magenta, and blue circles are for events recorded by the PIA, OPA, and KPA sites, respectively. The red triangles from south to north indicate the location of the PIA, OPA, and KPA sites, respectively. (For interpretation of the references to colour in this figure legend, the reader is referred to the web version of this article.)

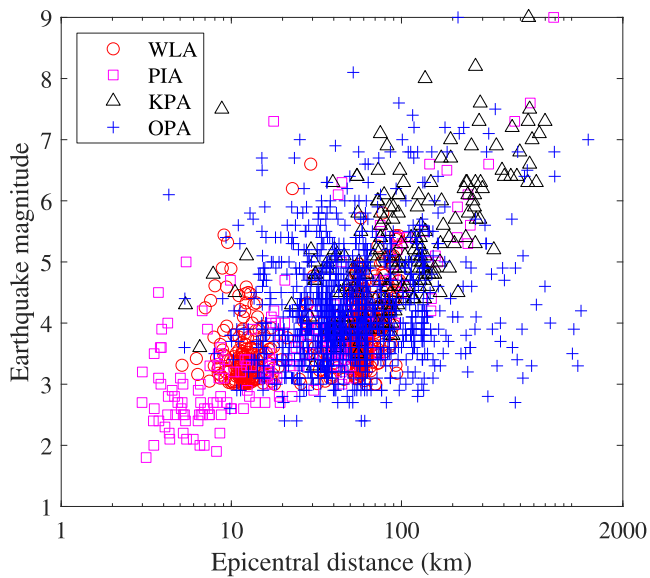


**Fig. A3.** Correlation between earthquake magnitude and epicentral distance of the ground motion recordings at the four sites.

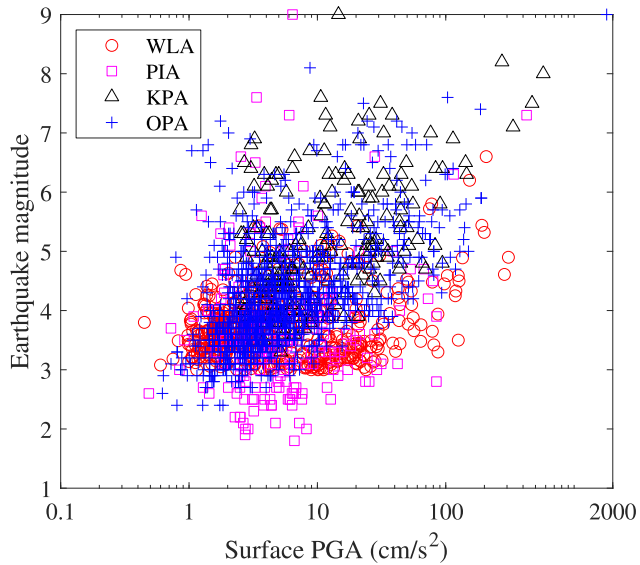


**Fig. A4.** Correlation between earthquake magnitude and surface peak ground acceleration of the ground motion recordings at the four sites.

## References

- Aguirre, J., Irikura, K., 1997. Nonlinearity, liquefaction, and velocity variation of soft soil layers in Port Island, Kobe, during the Hyogo-ken Nanbu earthquake. *Bull. Seismol. Soc. Am.* 87 (5), 1244–1258.
- Aki, K., 1993. Local site effects on weak and strong ground motion. *Tectonophysics* 218, 93–111.
- ASCE, 2017. ASCE 7-16: Minimum Design Loads for Buildings and Other Structures Commentary. American Society of Civil Engineers, Reston, VA.
- Bayless, J., Abrahamson, N.A., 2019. An empirical model for the interfrequency correlation of epsilon for Fourier amplitude spectra. *Bull. Seismol. Soc. Am.* 109 (3), 1058–1070.
- Bennett, M., McLaughlin, P., Sarmiento, J., Youd, T., 1984. Geotechnical investigation of liquefaction sites, Imperial Valley, California. In: US Geological Survey Open File Report 84-252. U.S. Geological Survey, Menlo Park, California 94025.
- Bonilla, L.F., Archuleta, R.J., Lavallée, D., 2005. Hysteretic and dilatant behavior of cohesionless soils and their effects on nonlinear site response: field data observations and modeling. *Bull. Seismol. Soc. Am.* 95 (6), 2373–2395.
- Bonilla, L.F., Tsuda, K., Pulido, N., Régnier, J., Laurendeau, A., 2011. Nonlinear site response evidence of KNET and KiK-net records from the Mw 9 Tohoku earthquake. *Earth Planets Space* 58, 1–7.
- Boulanger, R., Kamai, R., Ziotos, K., 2011. Numerical modeling of liquefaction effects. In: Proceeding of the Effects of Surface Geology on Seismic Motion, 4th IASPEI/IAEE International Symposium, Santa Barbara, California, pp. 23–26.
- Castro-Cruz, D., Régnier, J., Bertrand, E., Courboulex, F., 2020. A new parameter to empirically describe and predict the non-linear seismic response of sites derived from the analysis of Kik-Net database. *Soil Dyn. Earthq. Eng.* 128, 105833.
- Chávez-García, F.J., Kang, T.-S., 2014. Lateral heterogeneities and microtremors: limitations of HVSR and SPAC based studies for site response. *Eng. Geol.* 174, 1–10.
- Cultrera, G., Boore, D.M., Joyner, W.B., Dietel, C.M., 1999. Nonlinear soil response in the vicinity of the Van Normal complex following the 1994 Northridge, California, earthquake. *Bull. Seismol. Soc. Am.* 89 (5), 1214–1231.
- Derras, B., Bard, P.-Y., Régnier, J., Cadet, H., 2020. Non-linear modulation of site response: sensitivity to various surface ground-motion intensity measures and site-condition proxies using a neural network approach. *Eng. Geol.* 269, 105500.
- Dhakal, Y.P., Kunugi, T., Kimura, T., Suzuki, W., Aoi, S., 2019. Peak ground motions and characteristics of nonlinear site response during the 2018 Mw 6.6 Hokkaido eastern Iburi earthquake. *Earth Planets Space* 71 (1), 56.
- Elgamal, A.-W., Zeghal, M., Parra, E., 1996. Liquefaction of reclaimed island in Kobe, Japan. *J. Geotech. Eng.* 122 (1), 39–49.
- Frankel, A.D., Carver, D.L., Williams, R.A., 2002. Nonlinear and linear site response and basin effects in Seattle for the M 6.8 Nisqually, Washington, earthquake. *Bull. Seismol. Soc. Am.* 92 (6), 2090–2109.
- Gingery, J.R., Elgamal, A., Bray, J.D., 2015. Response spectra at liquefaction sites during shallow crustal earthquakes. *Earthquake Spectra* 31 (4), 2325–2349.
- Higashi, S., Matsutani, T., 2000. Nonlinear site response in Kushiro during the 1994 Hokkaido Tohoku-oki earthquake. *Bull. Seismol. Soc. Am.* 90 (4), 1082–1095.
- Holzer, T., Hanks, T., Youd, T., 1989. Dynamics of liquefaction during the 1987 Superstition Hills, California, earthquake. *Science* 244 (4900), 56–59.
- Iai, S., Matsunaga, Y., Morita, T., Miyata, M., Sakurai, H., 1994. Effects of remedial measures against liquefaction at 1993 Kushiro-Oki Earthquake. In: Technical Report NCEER, 94. US National Center for Earthquake Engineering Research (NCEER), pp. 135–152.
- Iai, S., Morita, T., Kameoka, T., Matsunaga, Y., Abiko, K., 1995. Response of a dense sand deposit during 1993 Kushiro-Oki earthquake. *Soils Found.* 35 (1), 115–131.
- Kaklamanos, J., Bradley, B.A., Thompson, E.M., Baise, L.G., 2013. Critical parameters affecting bias and variability in site-response analyses using KiK-net downhole array data. *Bull. Seismol. Soc. Am.* 103 (3), 1733–1749.
- Kishida, T., Tsai, C.-C., 2021. Wave velocities depending on shear strain, directionality, and excess pore water pressure from Wildlife Liquefaction Array. *Bull. Earthq. Eng.* 19 (6), 2371–2388.
- Ko, Y.-Y., Chen, C.-H., 2020. On the variation of mechanical properties of saturated sand during liquefaction observed in shaking table tests. *Soil Dyn. Earthq. Eng.* 129, 105946.
- Konno, K., Ohmachi, T., 1998. Ground-motion characteristics estimated from spectral ratio between horizontal and vertical components of microtremor. *Bull. Seismol. Soc. Am.* 88 (1), 228–241.
- Kostadinov, M.V., Yamazaki, F., 2001. Detection of soil liquefaction from strong motion records. *Earthq. Eng. Struct. Dyn.* 30 (2), 173–193.
- Kramer, S.L., Asl, B.A., Ozener, P., Sideras, S.S., 2015. Effects of liquefaction on ground surface motions. In: Perspectives on Earthquake Geotechnical Engineering. Springer, pp. 285–309.
- Kramer, S., Sideras, S., Greenfield, M., 2016. The timing of liquefaction and its utility in liquefaction hazard evaluation. *Soil Dyn. Earthq. Eng.* 91, 133–146.
- Kramer, S.L., Sideras, S.S., Greenfield, M.W., Hushmand, B., 2018. Liquefaction, ground motions, and pore pressures at the Wildlife Liquefaction Array in the 1987 Superstition Hills earthquake. In: Geotechnical Earthquake Engineering and Soil Dynamics V: Liquefaction Triggering, Consequences, and Mitigation. American Society of Civil Engineers Reston, VA, pp. 384–402.
- Power, M., Chiou, B., Abrahamson, N., Bozorgnia, Y., Shantz, T., Roblee, C., 2008. An overview of the NGA project. *Earthquake Spectra* 24 (1), 3–21.
- Rathje, E.M., Kottke, A.R., Trent, W.L., 2010. Influence of input motion and site property variabilities on seismic site response analysis. *J. Geotech. Geoenviron.* 136 (4), 607–619.
- Régnier, J., Cadet, H., Bonilla, L.F., Bertrand, E., Semblat, J.-F., 2013. Assessing nonlinear behavior of soils in seismic site response: statistical analysis on KiK-net strong-motion data. *Bull. Seismol. Soc. Am.* 103 (3), 1750–1770.
- Régnier, J., Cadet, H., Bard, P.-Y., 2016. Empirical quantification of the impact of nonlinear soil behavior on site response. *Bull. Seismol. Soc. Am.* 106 (4), 1710–1719.
- Ross, Z.E., Meier, M.-A., Hauksson, E., Heaton, T.H., 2018. Generalized seismic phase detection with deep learning. *Bull. Seismol. Soc. Am.* 108 (5A), 2894–2901.
- Roten, D., Fäh, D., Bonilla, L.F., 2013. High-frequency ground motion amplification during the 2011 Tohoku earthquake explained by soil dilatancy. *Geophys. J. Int.* 193 (2), 898–904.
- Sgarlato, G., Lombardo, G., Rigano, R., 2011. Evaluation of seismic site response nearby underground cavities using earthquake and ambient noise recordings: a case study in Catania area, Italy. *Eng. Geol.* 122 (3–4), 281–291.
- Steidl, J.H., Civilini, F., Seale, S., 2014. What have we learned after a decade of experiments and monitoring at the NEES@UCSB permanently instrumented field sites. In: Proceeding of the 10th US National Conference on Earthquake Engineering, pp. 21–25.
- Thabet, M., Nemoto, H., Nakagawa, K., 2008. Variation process in stiffness inferred by nonlinear inversion during mainshocks at Kushiro Port vertical array site. *Earth Planets Space* 60 (6), 581–589.
- Tsai, C.-C., Hwang, Y.-W., Lu, C.-C., 2020. Liquefaction, building settlement, and residual strength of two residential areas during the 2016 southern Taiwan earthquake. *Acta Geotech.* 15 (6), 1363–1379.

- Wen, K., Huang, J., Chen, C., Cheng, Y., 2011. Nonlinear site response of the 2010 Darfield, New Zealand earthquake sequence. In: 4th IASPEI/IAEE International Symposium: Effects of Surface Geology on Seismic Motion.
- Yamazaki, F., Ansary, M., Towhata, I., 1995. Application of a dynamic effective stress model at a reclaimed site during the Great Hanshin earthquake, 1995. In: Earthquake Geotechnical Engineering, pp. 591–597.
- Yang, J., Yan, X., 2009. Factors affecting site response to multi-directional earthquake loading. *Eng. Geol.* 107 (3–4), 77–87.
- Yang, J., Sato, T., Li, X.-S., 2000. Seismic amplification at a soft soil site with liquefiable layer. *J. Earthq. Eng.* 4 (01), 1–23.
- Youd, T.L., 2005. Lessons learned and need for instrumented liquefaction sites. In: Geomechanics: Testing, Modeling, and Simulation, pp. 504–523.
- Youd, T.L., Carter, B.L., 2005. Influence of soil softening and liquefaction on spectral acceleration. *J. Geotech. Geoenviron.* 131 (7), 811–825.
- Zorapapel, G.T., Vucetic, M., 1994. The effects of seismic pore water pressure on ground surface motion. *Earthquake Spectra* 10 (2), 403–438.